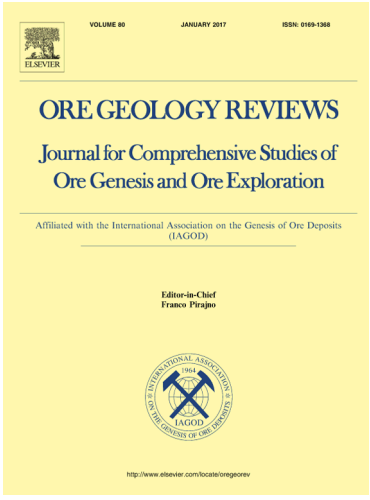

The sources of mineralizing fluids of orogenic gold deposits of the Baikal-Patom and Muya areas, Siberia: constraints from the C and N stable isotope compositions of fluid inclusions

Vsevolod Yu. Prokofiev, Yuri G. Safonov, Volker Lüders, Andrei A. Borovikov, Aleksey A. Kotov, Tatiana M. Zlobina, Konstantin Yu. Murashov, Marina A. Yudovskaya, Sofiya L. Selektor

PII: S0169-1368(18)30568-7
DOI: https://doi.org/10.1016/j.oregeorev.2019.102988
Article Number: 102988
Reference: OREGEO 102988

To appear in: *Ore Geology Reviews*

Received Date: 4 July 2018
Revised Date: 17 June 2019
Accepted Date: 24 June 2019

Please cite this article as: V. Yu. Prokofiev, Y.G. Safonov, V. Lüders, A.A. Borovikov, A.A. Kotov, T.M. Zlobina, K. Yu. Murashov, M.A. Yudovskaya, S.L. Selektor, The sources of mineralizing fluids of orogenic gold deposits of the Baikal-Patom and Muya areas, Siberia: constraints from the C and N stable isotope compositions of fluid inclusions, *Ore Geology Reviews* (2019), doi: https://doi.org/10.1016/j.oregeorev.2019.102988

The sources of mineralizing fluids of orogenic gold deposits of the Baikal-Patom and Muya areas, Siberia: constraints from the C and N stable isotope compositions of fluid inclusions

Vsevolod Yu. Prokofiev[1*], Yuri G. Safonov[1], Volker Lüders[2], Andrei A. Borovikov[3], Aleksey A. Kotov[1], Tatiana M. Zlobina[1], Konstantin Yu. Murashov[1], Marina A. Yudovskaya[1], and Sofiya L. Selektor[4].

[1]Institute of Geology of Ore Deposits, Petrography, Mineralogy and Geochemistry, Russian Academy of Sciences, Staromonetny per. 35, Moscow, 119117 Russia

[2]GFZ German Research Centre for Geosciences, Telegrafenberg, 14473 Potsdam, Germany

[3]V.S. Sobolev Institute of Geology and Mineralogy SB RAS; Novosibirsk, Russia

[4]Frumkin Institute of Physical Chemistry and Electrochemistry, Moscow 119071, Russia

*Corresponding author: vpr2004@rambler.ru

ABSTRACT

The compositions of fluid inclusions in quartz and sphalerite from five gold deposits of the Baikal-Patom (Sukhoi Log, Verninsk and Dogaldyn) and Baikal-Muya (Uryakh and Irokinda) foldbelts in the northern margin of the Central Asian Orogenic Belt, along its boundary with the Siberian craton, indicate that the gold mineralization was formed predominantly from heterogeneous CO_2-H_2O orogenic fluid. All deposits are structurally controlled and composed of veinlet-disseminated and vein to stockwork types of ores that are hosted by rocks that underwent regional metamorphism to the greenschist facies in Baikal-Patom and up to the granulite facies in Baikal-Muya. The gold-quartz veins of all the Baikal-Patom deposits and the Uryakh were formed by fluids of similar composition with salinity of 1.4-9.5 wt % NaCl equiv. and CO_2 content of 1.4-8.6 mol/kg of solution, under comparable physical conditions, at temperatures of 128-385 ºC and pressures of 570-3290 bar. Fluids of the granulate-hosted Irokinda deposit are distinguished for the highest temperatures and pressures and involve relics of medium- to high-temperature (179-453ºC) brines with salinity of 4.6-46.3 wt % NaCl equiv. The temperature and pressure of the mineralizing fluid increase roughly from north to south, which correlates with the increase in the metamorphic grade of the host rocks. The increase is accompanied by the simultaneous systematic shift in the C isotope composition of CO_2 (released from the quartz by the chrush-leach method) from –1.9 to –5.5 ‰ $\delta^{13}C_{CO2}$ in the Baikal-Patom and Uryakh from –0.6 to + 0.7 ‰ $\delta^{13}C_{CO2}$ at Irokinda. The C and N isotope compositions of CO_2 suggest that Irokinda fluids were partly derived from decarbonated marine limestone, whereas the orogenic gold-bearing fluids of the other deposits are interpreted to have been composed mostly of fluid from a crustal magmatic (granitic?) source.

Key word: Orogenic gold deposits, fluid inclusions, carbon isotopes, CO_2, Baikal-Patom foldbelt, Muya foldbelt.

1. Introduction

The Baikal-Patom and the Muya areas (Fig. 1) north of Lake Baikal are among Russia's largest gold mining areas, in which placer gold was mining starting in the 19th century and which attracted attention of many researchers (e.g. Buryak, 1982; Distler et al., 1996; Wood and Popov, 2006; Rusinov et al., 2008; Yakubchuk et al., 2014). Since the placer gold reserves tend to be exhausted, vein- and stockwork-type primary gold deposits hosted by clastic rocks become the leading gold producers.

Sukhoi Log is the most famous and largest deposit in Baikal-Patom. It is the best-studied gold deposit in the area and has been intensely studied since its discovery in 1961 (e.g. Laverov et al., 2000; Distler et al., 2004; Large et al., 2007; Kryazhev et al., 2009; Dubinina et al., 2014). However, the genesis of Sukhoi Log, as well as other smaller deposits of the area, is still highly debatable. There are two fundamentally different hypotheses for the sources of the gold. The first one (metamorphic-sedimentary) implies gold leaching from crustal rocks with an elevated or ordinary metal background concentrations and its focused re-deposition during metamorphism (e.g. Nemerov, 1989; Buryak and Khmelevskaya, 1997; Large et al., 2007). The other hypothesis suggests that the gold mineralization is related to an inflow of gold-bearing fluids from deep-seated lower crustal or mantle sources (Sher, 1972; Rundqvist et al., 1992; Distler et al., 1996; Lishnevsky, Distler, 2004; Safonov, 2006; Mitrofanov, 2006; Kucherenko et al., 2011; Yudovskaya et al., 2016). There are a number of transitional models that try to reconcile the shortages of the major hypothesis and to link the Sukhoi Log-type mineralization with the complex and multistage geological history of the region (Meffre et al., 2008; Kryazhev et al., 2009, Yudovskaya et al., 2011; Yakubchuk et al., 2014, among many others). The classification of the deposits as orogenic ones (Groves et al., 1998; Goldfarb et al., 2005; 2014) is based mainly on their structurally-controlled local setting and the high P-T parameters of their mineralizing fluids, albeit the geochronological constraints also strongly support the superimposed character of mineralization.

We have studied fluid inclusions in quartz and sphalerite from five gold deposits located within the neighboring Baikal–Patom and Baikal–Muya belts (Fig. 1). The gold reserves of the studied deposits range from very large (>1000 t Au), large (100 to 300 t Au) to medium-sized and small (10–20 t Au). This study was focused on determining the physicochemical parameters

of mineralizing fluids at the gold deposits of various scales and om conducting a comparative analysis of the data to identify favorable characteristics of highly-endowed gold-bearing fluids.

2. Geological setting

Three of the studied gold deposits, including Sukhoy Log, Verninsk and Dogaldyn, are located with the Mama-Bodaibo basin in the central part of the Baikal–Patom fold-and-thrust belt that spatially coincides with the boundaries of the Lena gold province (Fig. 2). The Baikal–Vitim–Barguzin and the Baikal–Muya foldbelts, as well as the Barguzin Superterrane, are thought to be neighboring accretionary terrains, which share a geological history starting from the Neoproterozoic (e.g Yarmolyuk et al., 2006; Rytsk et al., 2011). Two of the studied gold deposits, the Uryakh and the Irokinda, are located in the Muya gold district in the eastern margin of the Baikal-Muya foldbelt (Fig. 2). The geological evolution of these terrains is related to the evolution of the Central Asian Orogenic Belt (CAOB), one of the world's largest accretionary orogens (Kröner et al., 2014) that was produced by the multi-stage collision of the Siberian, Tarim and North China cratons (Yarmolyuk et al., 2006; Rytsk et al., 2011). The Baikal–Patom foldbelt is considered to have developed mostly as a passive continental margin of the Siberian craton whereas the Baikal-Muya belt is one of the CAOB earliest collisional terrains composed of ophiolitic and island-arc complexes (Bulgatov and Gordienko, 1999; Skuzavatov et al., 2019). Therefore, the gold deposits of the Baikal-Patom foldbelt were formed in a geological and geodynamic framework different from those of gold-quartz deposits of the Baikal-Muya block.

2.1 Deposits of the Baikal-Patom foldbelt

The geological description of the Sukhoi Log deposit is given in several earlier and recent papers (e.g. Distler et al., 1996, 2004; Yudovskaya et al., 2016 and references therein). The most comprehensive characteristics of the Baikal-Patom geological sequences are given in the collective monograph “The Precambrian of the Patom Highland” published in Russian (Ivanov et al., 1995). Data from it are mostly referred to below.

The Sukhoi Log, Verninsk and Dogaldyn deposits are hosted by metamorphosed terrigenous black shales to sandstones of the Neoproterozoic sequences within the Bodaibo Synclinorium (Fig. 2). Geochronological data indicate that the deposition of the host sedimentary rocks started in the early Ediacaran and ended prior to an age of ~520 Ma, with the younger formations straddling the Ediacaran-Cambrian boundary (see the summary in Yudovskaya et al., 2016). A Rb-Sr whole-rock isochron age of 447± 6 Ma for the host metashales of Sukhoi Log (Laverov et al., 2007), a U-Th-Pb isotopic age of 440-460 Ma for the newly-formed crystalline monazite and zircon (Yudovskaya et al., 2011), and a roughly coeval Re-Os isochron age of the

ore sulfides are interpreted to be the age of metamorphism and related syn- and post-metamorphic mineralization. A Rb-Sr isotopic age of 321± 14 Ma for vein quartz (Laverov et al., 2007) and similar U-Th-Pb isotopic ages of hydrothermal monazite (Meffre et al., 2008) are believed to reflect the influence of the plume-related multiphase Angara-Vitim magmatic event (Tsygankov et al., 2007).

All gold deposits within the Bodaibo Synclinorium are confined to the axial zone of the northeast trending Patom–Vilyui paleorift. Safonov (2006) suggested that the west-northwest trend of the mineralization, which seems to be typical of all deposits and occurrences of the area, is defined by transform normal faults related to the mosaic-block structure of the paleorift. Conversely, according to local exploration interpretations, it is the local west-east fold-thrust system that dominantly controls the ore mineralization (Ivanov et al., 1995).

The Sukhoi Log deposit is confined to the axial part of an overturned anticline that occurs within the larger high-order Marakan-Tunguska syncline (Fig. 3). The axial plane of the fold coincides with a fault, which is as a zone of both ductile deformation and cataclasis. The thickness of host shale of the Ediacaran Khomolkho Formation is significantly reduced in the core of the fold in comparison to its flanks. Numerous minor plicative structures of different scale are selectively developed in the fine-grained metashales, whereas the rigid sandstones and quartz-sulfide aggregates show brittle deformation and boudinage.

The Verninsk deposit is also confined to an overturned anticline complicated by a sub-latitudinal shallow dipping thrust. The orebody is hosted in metamorphosed black shales and sandstones with minor limestones of the Ediacaran Aunakit Formation. The anticline is complicated by numerous plicative and brittle structures of several orders, including a number of sub-parallel minor thrusts, which are generally parallel to the major thrust (Fig. 3).

The Dogaldyn (or Dogaldyn Zhila, which means *Dogaldyn Vein* in Russian) deposit is constrained within the Dogaldyn thrust zone. It consists of a single 15 km-long quartz vein crosscutting metamorphosed shales of the Dogaldyn Formation, one of the topmost Neoproterozoic stratigraphic units, which also hosts several other small gold deposits and occurrences (Fig. 3).

The orebodies of the Sukhoi Log and Verninsk deposits include superimposed zones of veinlet, stockworks and disseminated types of quartz-sulfide mineralization (Fig. 4). The outlines of the orebodies are defined in terms of off-cut grades. Along with the main veinlet-disseminated bodies, both deposits contain massive quartz veins that are controlled by roughly E–W trending steeply (50º-70º) dipping fault zones. The high-grade parts of the Sukhoi Log quartz veins were developed in the 19th century, whereas the remaining veins of the so-called Central vein zone

show a poor grade. The massive quartz veins of the Verninsk deposit also form the similar steeply-dipping Pervenets vein orebody, which locally contains conditional mineralization.

The mineralization is dominated by native gold in association with quartz, sulfides and carbonates (dolomite and ankerite), although the ore also contains a long list of minor and accessory minerals (Distler et al., 2004). The Sukhoi Log and Verninsk deposits contain mineralization of two types: qold-quart-sulfide veinlet-disseminated and gold-quartz veins. The gold is predominantly associated with several generations of pyrite, minor pyrrhotite and arsenopyrite in Sukhoi Log ores, whereas arsenopyrite and pyrite are major sulfides in the Verninsk deposit (Fig. 5). Mineralisation of the Dogaldyn deposit is composed of gold–quartz–sphalerite–galena assemblages with minor arsenopyrite and pyrite ± chalcopyrite, whose amount increases with depth.

The reserves of the deposits are estimated as follows:

– Sukhoi Log: 1500 tonnes Au with average grade of 2.73 g/t (Migachev et al., 2008);

– Verninsk: 180 tonnes Au with average grade of 2.7 g/t (Polyus Gold Press Release, 2015);

– Dogaldyn– 18 tonnes Au with average grade of 1.7 g/t (Ivanov, 2014).

2.2 The deposits of the Baikal-Muya foldbelt

The Uryakh and Irokinda deposits are located at a distance of 160 km from each other in the eastern part of the Baikal–Muya foldbelt, close to the boundary with the southwestern margin of the Aldan–Stanovoy ancient block of the Siberian Craton (Figs. 2 and 6).

The Uryakh mineralization is spatially controlled by the steeply westward-dipping Syulban deep-seated fault zone. The host rocks of Ediacaran age volcanic rocks of the Ust-Kelyana Formation, black shales of the Vodorazdel Formation and limestones of the Ust-Uryakh Formation. The Ediacaran host sequences are intruded by gabbroic and plagiogranite dykes and stocks, which occur as lenses and chains of bodies concordant to the faults and general beddings. All rocks are metamorphosed to the greenschists to amphibolite facies and are transformed into blastomylonites and cataclasytes in the vicinities of faults. The oldest granitoid complexes have supposedly Paleoproterozoic to Ediacaran ages, whereas the youngest dykes are ascribed to the Late Paleozoic Kadali-Butuin and Kachoi complexes (Fig. 6).

The quartz–gold–silver–sulfide stockwork and vein mineralization (Fig. 4) extends over a distance of 12 km along the major Syulban fault. The block structure of the deposit resulted from tectonic motions along two duplex systems: the major Syulban fault and a related transverse second-order fault system. The ore-hosting structures vary from stockworks to linear veins and veinlet zones (Zlobina et al., 2016). Some newly formed mineralization is overprinted on the

youngest dolerite dykes. A Rb-Sr whole-rock isochron age of 281± 5 Ma for the mineralized beresite metasomatites is identical, within the uncertainties, to the Ar-Ar plateau age of 275 ± 6 Ma for the same rocks (Chugaev et al., 2015). Therefore, the gold mineralization event is coeval to the youngest granite phase of the giant Angara-Vitim batholith (Tsygankov et al., 2007), whose intrusions are exposed north to the Uryakh orefield.

The sulfide assemblage makes up < 0.5-2.5 % of the vein mineralization and consists of major pyrite, chalcopyrite, sphalerite, galena, and minor arsenopyrite, fahlore and pyrrhotite (Fig. 5). The noble metal minerals are native gold, Au-Ag alloys, native silver, and minerals of the acanthite–argentite group.

The Irokinda gold-quartz vein deposit is constrained to the so-called Muya block, which is a cratonic-basement high surrounded by diverse Proterozoic rocks of the Baikal–Muya belt close to the boundary with the eastern margin of the Siberian platform (Fig. 2). The Muya block is bordered by the E–W-trending Northern and Southern Muya deep faults in the south and north and by long-lived mobile zones in the west and east (Fig. 6). The mineralization is hosted mostly by ancient highly metamorphosed rocks, such as gneiss, migmatites, amphibolites, schists and marbles. The high-grade transformation of Muya rocks resulted from repeated metamorphic events in the Tonian (764–754 Ma) and Ediacaran (622–608 Ma) (Skuzovatov et al., 2019), whereas the age of the sedimentary protolith is highly debatable but is likely no older than ~1 Ga, as follows from the zircon U-Pb and Nd-Hf isotope data (Skuzovatov et al., 2019). The younger host rocks are weakly metamorphosed Early Neoproterozoic plutonic and volcanic rocks and Paleozoic granitic, dioritic and doleritic dykes. The ore-bearing veins are confined to the lying side of the Vostochny Fault of the Kelyana fault zone. The veins fill the north-east to north-northwest branching fractures and minor faults; and the vein distribution is also locally controlled by low-angle dynamometamorphic schist zones that extends for several hundred meters to several kilometers. The veins in the schist zones are discontinuous, show a linear or S-shaped morphology (Fig. 4) and locally form up to a 1200 m-thick packages of the differently oriented veins to stockwork (Zlobina et al., 2014).

The gold occurs in the carbonate–sulfide–quartz veins as native gold and, to some extent, as "invisible" gold in pyrite. The gold distribution is highly heterogeneous, and grade of the ores varies from an off-cut to over 1000 g/t Au. The orebody also includes veinlets and networks of superimposed younger gold-sphalerite-galena mineralization with rare chalcopyrite, pyrrhotite, arsenopyrite, and fahlore (Fig. 5). The total sulfide content is < 0.5 wt. %.

Gold resources of the studied deposits are estimated at:

– Uryakh: 56 tonnes Au (Ivanov, 2014) with an average grade of 4.3 g/t Au;

– Irokinda: >60 tonnes Au (Ananin et al., 2000) with an average grade of 4.7 g/t Au.

3. Methods

Fluid inclusions were studied in quartz samples from veins and veinlets of all gold deposits under review. For this purpose doubly-polished 0.3-0.5 mm thick sections were prepared from quartz samples for optical, thermometric, and cryometric studies of fluid inclusions. Fluid inclusions were studied using a Olympus BX51 optical microscope. Microthermometric measurements were performed with a THMSG-600 heating stage (Linkam, United Kingdom). The salt components in the inclusions were derived from eutectic temperatures (Borisenko, 1977). Fluid salinity was determined from ice melting temperatures in two-phase inclusions and/or from homogenization temperatures of halite daughter crystals in multi-phase inclusions, all modelled in terms of the NaCl–H_2O system (Bodnar and Vityk, 1994). Fluid salinity in carbon dioxide–water inclusions was estimated from gas hydrate melting temperatures (Collins, 1979). Carbon dioxide concentrations in solutions were calculated from the volume and weight ratios of fluid components (Prokof'ev and Naumov, 1987). To calculate the proportions of phase volumes in inclusions of the regular shape, the linear dimensions of the fluid inclusion and the phase of liquid CO_2 were measured (in three axes, using Fedorov's table). The volumes of fluid inclusion and the phase of liquid CO_2 were calculated according the formulas for the volume of an ellipsoid or a sphere.

In cases where minerals contained co-genetically trapped carbon dioxide–water and CO_2 gas inclusions, pressure was determined from the intersection of the isochores, calculated on gas inclusions, and the line of homogenization temperature of carbon dioxide-water inclusions (Kalyuzhny, 1982). Fluid inclusions that trapped coexisting heterogeneous fluids within the two-phase equilibrium line, do not require pressure corrections and, homogenized at the highest temperature (Roedder, 1984). The average temperature of homogenization of carbon dioxide-water inclusions was determined from the groups of fluid inclusions with the same phase relationships and the same homogenization temperature. The composition of the inclusions in this group corresponds to the composition of the aqueous phase of the heterogeneous fluid. Fluid inclusions with variable phase ratios that trapped different phases of the heterogeneous fluid were excluded from consideration. Fluid inclusion data for CO_2-CH_4-N_2 gas were interpreted with reference to the published literature (Kerkhof, 1988 and Thiery et al., 1994).

Salt concentration, fluid density, and fluid pressure were calculated using the FLINCOR software (Brown, 1989).

Aqueous and gas extracts from fluid inclusions were analyzed on a 0.5 g sample of 0.50–0.25 mm size fraction) using the technique described by Kryazhev et al. (2006). The basic flow

sheet of the bulk analysis of fluid inclusions included sample cleaning, fluid inclusions breaching, and determination of the composition of the released components by various methods. The sample was cleaned first with 50 vol. % (1+1) HNO_3 solution and then exposed to electrolytic cleaning in a water flow using an ultrasonic bath. The dried sample was placed into a disposable glass reactor, which was vacuumed at 110°C and filled with helium. A crushing stage enabled fluid inclusions to be breached mechanically or thermally depending on the problem to be solved. Thermal breaching was performed by heating up to 400°C. Mechanical breaching was carried out by means of small corundum balls and a vibrator at a temperature of 120°C in order to suppress gas sorption and to permit quantitative analysis of H_2O. The released gases were fed by a dosing valve into a TSVET-100 gas chromatograph equipped with a flow divider for the simultaneous determination of H_2O, CO_2, CH_4, and other gases. The reactor with the crushed (or decrepitated) sample was filled with deionized water (7 ml) and placed in an ultrasonic bath for 15 min. The extracted solution was separated by centrifuging and subjected to ion chromatography on the TSVET-3006 liquid chromatograph to determine Cl^-, F^-, SO_4^{2-}, and HCO_3^-– concentrations with a detection limit of 0.01 mg/l and to ICP mass spectrometry on an Elan 6100 device, for other components. Thus, gases, salts, and the solvent (water) were extracted simultaneously from bulk fluid inclusion samples during analysis, enabling reliable calculation of concentrations in solutions. Minimization of the number of analytical operations reduced the probability of sample contamination with foreign admixtures in the course of analysis. The standardization procedure ensured highest possible error compensation and raised the reliability of detected differences between fluid compositions of the studied sample series. The data on blank extracts were subtracted from the results obtained. The remaining useful signal represents the contents of fluid inclusions with a high probability. Therefore, we may conclude that bulk analysis data reflect the bulk concentrations of fluid inclusion components.

Compositions of the gas and solid phases in individual fluid inclusions were studied by Raman spectroscopy using a Jobin Yvon LabRAM HR800 spectrometer.

The carbon isotopic compositions of fluid inclusion gases were measured at the GFZ Potsdam, Germany using a sample crusher, GC-column, EA, a ConFloIII interface and a Thermo DeltaplusXL mass spectrometer according to the online method described by Plessen and Lüders (2012). Variations in $\delta^{13}C$ values of CO_2 of quartz-hosted gas-rich fluid inclusion assemblages in previously studied quartz chips from the Ashanti gold mine (GH-172 and GH-151, Plessen and Lüders (2012) show excellent reproducibility in the range between 0.5 and 0.4‰, respectively.

4. Fluid inclusion characteristics

4.1. Sampling

This study presents data on fluid inclusions (FI), which are hosted mostly in quartz, from ore veins and veinlets sampled in the mines (Fig. 4). Mineral paragenetic sequence of the main ore stage for the studied deposits is compiled based on the previous studies (Distler et al., 1996, 2004; Yakubchuk et al., 2014) and our observations and shown in Figure 5. Quartz from the veins and veinlets underwent partial recrystallization and deformation, and because of this only about 10 % of our thin sections contain FI suitable for thermometric experiments. For the Sukhoi Log deposit, 23 borehole samples of gold-sulfide-quartz ores were studied. For the Verninsk deposit, 5 samples of gold-bearing quartz were taken from an open pit and exploration trenches. Six samples were collected from an adit and trenches at the Digaldyn deposit. The Uryakh mineralization was represented by samples form five borehole, and 10 Irokinda ore samples were collected in underground mines. Visible grains of native gold were found in most of the studied quartz samples (Fig. 7).

4.2. Description of the fluid inclusions

Fluid inclusions 2-25 μm have variable morphologies, including irregular ones and those of negative crystals. In terms of phase composition at the room temperature, the following four types of FI are distinguished (Fig. 8): type 1 (CO_2-aqueous) is two- or three-phase CO_2-aqueous inclusions; type 2 (V) is predominantly gas inclusions with liquid CO_2 (including subtype 2a inclusions with high-density nitrogen); type 3 (L-V) is two-phase inclusions containing aqueous solution and a gas bubble; and type 4 (L-V-S) is three- and multi-phase FI containing aqueous solution, a gas bubble and at least one up to several crystals with the largest cubic crystal, which were identified as halite based on its index of refraction. The type 2 (V) FI (Fig. 8e, f) were commonly trapped simultaneously with the type 1 CO_2-aqueous FI (Fig. 8a, b), likely indicating that the mineralizing fluid was heterogeneous. The type 1 and type 2 FI were found in quartz from all deposits, whereas the type 3 (L-V) FI occur in quartz from the Sukhoi Log, Verninsk, Uryakh and Irokinda deposits. The type 4 (L-V-S) FI were detected only in some quartz samples from the Irokinda deposit.

Quartz aggregates from the gold-bearing veins are composed of the equant or elongate, commonly heavily fractured grains. Cathodoluminescence reveals the presence of re-crystallised domains along the margins, whereas the cores of the grains are not re-crystallized. Most of the FI are confined to internal fractures. However, the central unfractured parts of the quartz grains sometimes enclose FI of types 1, 2 and 4 that are not related to any fractures. These inclusions are asserted to be the primary FI (P) (Fig. 9). The FI of types 1 and 2, as well as 4 and 2, often coexist with one another in quartz that reflect a heterogeneous state of the fluid and high concentrations of carbonic acid in it. Specifically, these FI trapped the fluid that was responsible

for gold precipitation. These FI are locally confined to zones of crystal growth that also confirm their primary origin (Fig. 9f).

The type 1 CO_2-aqueous FI in the internal fractures restricted to grain boundaries sometimes contain a phase of dense CO_2 of relatively small volume. These inclusions are referred to as pseudo-secondary (PS) FI, as compared to the secondary (S) L-V FI of aqueous-salt solutions that are mostly confined to fractures across the quartz grains.

4.3. Microthermometric data

Microthermometric data on more than 2000 individual fluid inclusions are shown, along with the calculated fluid densities and pressure of fluid entrapment, in Figure 10 and in Table 1. The type-1 CO_2-aqueous FI commonly decrepitate prior to homogenization at heating because of the high fluid pressure. Thereby homogenization temperature was determined only for several smaller inclusions within the studied association.

4.3.1. The Sukhoi Log deposit

Type 1 CO_2-aqueous FI exhibit homogenization temperatures of 210–385°C; fluid salinity of 5.0–8.1 wt% NaCl equiv; and CO_2 concentration of 1.8–7.6 mol/kg. The eutectic temperatures of –30 to –34°C suggest that Na, Mg, and Fe chlorides are the predominant solutes. The melting temperature of CO_2 in the gas phase of the type 1 CO_2-aqueous FI varies from –57.2 to –82.2°C. The fluid density is 0.82–1.09 g/cm^3.

The presence of carbon dioxide in FI follows from the physical properties: the critical temperature of +31.05°C and the triple point temperature of –56.6°C (Roedder, 1984). When subjected to supercooling (at –100°C) CO_2 freezes into numerous very small crystals, which is seen as FI darkening. These crystals subsequently merge into a solitary crystal that melts when heated above –56.6°C.

Carbon dioxide in the type 2 (V) FI homogenized into liquid at temperatures varying from –11.9 to +18.6°C. Its melting temperature varies from –57.0 to –60.8°C and noticeably differs from the melting point of pure CO_2 (–56.6°C), which is interpreted as caused by admixtures of gases with low boiling points CH_4 or N_2). The density of CO_2 is within 0.71–0.92 g/cm^3.

The subtype 2a (V) FI are filled with high-density gas mixture that unmixes at supercooling at temperatures below –160°C. This suggests the prevalence of nitrogen in the gas mixture. The homogenization temperatures of such inclusions vary from –153.5 (into gas) to –158.6°C (into liquids). Sporadic solid carbon dioxide with melting point varying from –62.3 to –83.5°C freezes out of the mixture. The density of the gas mixture is 0.12–0.57 g/cm^3.

The two-phase type 3 (L-V) FI homogenize into liquid at 130-385°C and contain aqueous solution with salinities of 3.7–9.5 wt% NaCl equiv. The predominant solutes in these inclusions

are also Na, Mg, and Fe chlorides (eutectic points of –25 to –34°C). The fluid density is 0.65–0.97 g/cm^3.

Therefore, gold-bearing mineralizing fluids of the Sukhoi Log contain high concentrations of CO_2 and other gases, and have a low salinity, which corresponds, based on their compositions, to the typical fluids at orogenic gold deposits (Ridley, Diamond, 2000) .

4.3.2. The Verninsk deposit

The type 1 CO_2-aqueous FI have homogenization temperatures of 252–356 °C; fluid salinity of 1.4–8.1 wt% NaCl equiv.; CO_2 concentration of 1.4–8.6 mol/kg. The eutectic points at –25 to –32°C suggest that the predominant solutes are Na, Mg, and Fe chlorides. The melting temperature of CO_2 in the gas phase of the type 1 CO_2-aqueous FI varies from –57.1 to –60.8 °C. Fluid density is 0.84–1.05 g/cm^3.

Carbon dioxide in the type 2 (V) FI homogenizes into liquid at temperatures varying from –13.7 to +30.8°C. Its melting point varies from –56.9 to –64.7°C and differs noticeably from the pure CO_2 melting point of –56.6°C, suggesting admixtures of gases with low boiling point (CH_4 or N_2). The density of CO_2 is 0.54–1.00 g/cm^3.

The low-temperature type 1 CO_2-aqueous PS FI have homogenization temperature of 179°C, fluid salinity of 5.0 wt% NaCl equiv., and CO_2 concentration of 2.3 mol/kg. The eutectic point of –31°C suggests the prevalence of Na, Mg and Fe chlorides in the solution. The melting point of CO_2 into gas is –58.0°C. The fluid density is 1.03 g/cm^3.

The two-phase type 3 (L-V) FI homogenize into liquid at 136–261°C and contain aqueous solution with salinity of 5.0–6.2 wt% NaCl equiv. The predominant solutes in these FI are also Na, Mg, and Fe chlorides as followed from eutectic points varying within a range from –26 to –33°C. The fluid density is 0.83–0.97 g/cm^3.

The PT parameters and compositions of the Verninsk ore-bearing fluids are closely similar to those of the Sukhoi Log and the other orogenic deposits (Ridley, Diamond, 2000).The indicative features are the high content of CO_2 and other gases as well as the low salinity.

4.3.3. The Dogaldyn deposit

The type 1 (CO_2-aqueous) FI have homogenization temperatures of 265–339°C; fluid salinity of 1.4–7.3 wt% NaCl equiv., and a CO_2 concentration of 2.6–7.1 mol/kg. The eutectic points of –30 to –39°C suggest that the predominant solutes are Na, Mg, and Fe chlorides. The melting point of carbon dioxide in the gas phase of the type 1 CO_2-aqueous FI varies from –56.8 to –60.2°C. The fluid density is 0.90–1.05 g/cm^3.

Carbon dioxide in the type 2 (V) FI homogenizes into liquid at temperatures varying from –14.1 to +22.1°C. Its melting point varies from –57.0 to –60.4°C and differs from the pure CO_2

melting point of –56.6°C, which is likely explained by the presence of CH_4 or N_2. The density of CO2 is 0.75–1.00 g/cm$_3$.

The type 1 (CO_2-aqueous) FI were also found in sphalerite. The sphalerite-hosted type FI have homogenization temperatures of 267–283°C, fluid salinity of 6.7 wt% NaCl eq, and CO_2 concentration of 3.7 mol/kg. The eutectic point of –39°C suggests the prevalence of Na, Mg, and Fe chlorides in the solution. The melting point of CO_2 in the gas phase is –60.2°C. The fluid density is 1.05 g/cm^3.

The low-temperature type 1 CO_2-aqueous PS FI are characterized by homogenization temperature of 128–236°C, fluid salinity of 3.7–7.3 wt% NaCl equiv., and CO_2 concentration of 1.7–2.9 mol/kg. The eutectic point (–29 to –30°C) suggests the prevalence of Na, Mg and Fe chlorides in the solution. The melting point of CO_2 in the gas phase was not determined because of the small sizes of the gas bubbles. The fluid density is 0.96–1.05 g/cm^3.

Ore-bearing fluids of the Dogaldyn are characterized by a high content of CO_2 and low salinity, which are typical of orogenic gold mineralization (Ridley, Diamond, 2000). The PT parameters of entrapment are close to those of the other deposits of the Baikal-Patom area.

4.3.4. The Uryakh deposit

The type 1 (CO_2-aqueous) FI have homogenization temperatures of 289–361°C; fluid salinity of 2.5–5.2 wt% NaCl equiv. and CO_2 concentration of 3.8–7.7 mol/kg.). Sodium, Mg, and Fe chlorides are the predominant solutes, as follows from the eutectic temperatures of –30 to–34°C. The melting point of CO_2 in the gas phase varies from –57.3 to –58.0°C, and the fluid density is 0.96–1.06 g/cm^3.

Carbon dioxide in the type 2 (V) FI homogenizes into liquid at temperatures ranging from –14.3 to +25.6°C. Its melting point varies from –57.0 to –59.1°C, indicating the presence of CH_4 or N_2. The density of CO_2 is 0.70–1.01 g/cm^3.

The low-temperature type 1 CO_2-aqueous PS FI with homogenization temperature of 213°C, fluid salinity of 5.2 wt% NaCl equiv., and a CO_2 concentration of 3.8 mol/kg were also found. The eutectic temperature of –30°C points out the prevalence of Na, Mg and Fe chlorides in the solution. The melting point of CO_2 in the gas phase of FI is –58.1°C and fluid density is 1.08 g/cm^3.

The two-phase type 3 L-V FI homogenize into liquid at 191°C and contain aqueous solution with salinities of 9.1 wt% NaCl equiv. The predominant solutes in these inclusions are also Na, Mg, and Fe chlorides based on eutectic temperature of –30°C. Fluid density is 0.94 g/cm^3.

Therefore, the ore-bearing fluid of the Uryakh deposits from the Baikal-Muya belt are similar to the mineralizing fluids of the Baikal-Patom deposits in terms of their compositions and

PT conditions. The fluids are characterized by a high CO_2 content and low salinity, which are the indicative features of orogenic gold mineralization (Ridley, Diamond, 2000).

4.3.5. The Irokinda deposit

The type 1 (CO_2-aqueous) FI have homogenization temperatures of 270–384°C; fluid salinity of 3.9–23.4 wt% NaCl equiv. and CO_2 concentration of 2.4–7.7 mol/kg. The eutectic points varies from –30 to –52°C and suggests that the predominant solutes are Na, Mg, and Ca chlorides. The melting point of CO_2 in the gas phase varies from –57.0 to –62.6°C, and the fluid density is 0.98–1.15 g/cm^3.

Carbon dioxide in the type 2 (V) FI homogenizes into liquid at temperatures varying from –32.4 to +27.5°C. Its melting point varies from –56.7 to –61.0°C, indicating admixtures of gases with low boiling points (CH_4 or N_2). The density of CO_2 is 0.67–1.09 g/cm^3.

The sphalerite contains type 1 (CO_2-aqueous) FI with homogenization temperature of 270°C, fluid salinity of 7.5 wt% NaCl equiv, and a CO_2 concentration of 1.5 mol/kg. The eutectic point (–32°C) suggests the prevalence of Na, Mg, and Fe chlorides in the solution. The melting point of CO_2 in the gas phase is –62.6°C. The fluid density is 1.09 g/cm^3.

The low-temperature type 1 (CO_2-aqueous) PS FI have a homogenization temperature of 191°C; fluid salinity of 8.5 wt% NaCl eq and CO_2 concentration of 1.5 mol/kg. The eutectic point of –36°C suggests the prevalence of Na, Mg and Fe chlorides in the solution. The melting point of CO_2 in the gas phase was not determined because of the small sizes of the gas bubbles. The fluid density is 1.06 g/cm^3.

The type 3 two-phase L-V FI homogenize into liquid at 172–230°C and contain aqueous solution with salinities of 11.7–18.9 wt% NaCl equiv. The predominant solutes in these inclusions are also Na, Mg and Ca chlorides (eutectic point –34 to –60°C). The fluid density is 0.97–1.03 g/cm^3.

Homogenization of the type 4 multiphase L-V-S FI in quartz with the complete dissolution of all daughter phases was reached at 320–453°C. Salt concentrations of the chloride brine vary within 39.8–46.3 wt% NaCl equiv. The brine is also dominated by Na, Mg and Ca chlorides, as follows from the eutectic points of –40 to –55°C. The fluid density is 1.02-1.13 g/cm^3.

The compositions and PT parameters of Irokinda auriferous fluids are different from those of the Sukhoi Log, Verninsk, Dogaldyn and Uryakh deposits. The presence of chloride brines distinguishes the latter from typical orogenic fluids as defined by Ridley and Diamond (2000), although the high abundances of CO_2 and other gases in the Irokinda inclusions are consistent with the orogenic style of the mineralization. We envisage that Irokinda fluids were derived from a reservoir different from the fluid source of the first four deposits.

The microthermometric study shows that quartz of all the studied deposits was formed from CO_2-rich fluids at the high pressure. The fluid pressure estimated by an isochoric P-T projection for the type 1 and type 2 fluid inclusions varies within a wide range (Fig. 11): Sukhoi Log 800-2630 bar (av. 1506 bar), Verninsk 570-2450 bar (av. 1828 bar), Dogaldyn 960-3230 bar (av. 1952 bar), Uryakh 1050-3290 bar (av. 2015 bar), Irokinda 840-5030 bar (av. 2360 bar). In general, both the average and the highest pressure values increase from northwest to southeast, from the Sukhoi Log deposit to the Irokinda deposit (Fig. 2). The increase in pressure is accompanied by an increase in temperatures: Sukhoi Log 210-385 ºC (av. 298 °C), Verninsk 246-356 ºC (av. 301 °C), Dogaldyn 265-339 ºC (av. 302 °C), Uryakh 289 -361 ºC (av. 325 °C), Irokinda 270-453 ºC (av. 362 °C).

4.4. Raman data

Results of Raman spectroscopic analysis of the molecular compositions of gas-bearing fluid inclusion are presented in Table 2.

For the Sukhoi Log deposit, the presence of 74.4–80.2 mol. % CO_2 and 19.7–25.6 mol. % N_2 in the type 2 (V) FI is confirmed by Raman spectroscopy.

For the Verninsk deposit, the presence of (mol. %) 77.7–98.4 CO_2, 1.6–22.2 N_2, 0.0-0.04 H_2S and 0.0-0.04 CH_4 is established in the type 1 (CO_2-aqueous) FI. The type 2 (V) FI contain (mol. %) 91.5–93.2 CO_2, 6.8–8.2 N_2 and 0.00-0.01 CH_4, according to the Raman spectroscopy data.

For the Dogaldyn deposit, Raman spectroscopy data attest to a presence of 98.2–99.0 mol. % CO_2 and nitrogen 1.0–1.8 mol. % N_2 in the type 2 (V) FI.

For the Uryakh deposit, Raman spectroscopy confirms the presence of 98.2 mol. % CO_2 and 1.8 mol. % N_2 in the type 1 (CO_2-aqueous) FI and 96.1 mol. % CO_2 and 3.9 mol. % N_2 in the type 2 (V) FI.

For the Irokinda deposit, 56.6–98.7 mol. % CO_2, 0.0–43.4 mol. % N_2 and 0.04-1.29 mol. % CH_4 are determined in the type-1 (CO_2- aqueous) FI. The type-2 (V) FI contain 75.9–99.7 mol. % CO_2, 0–24.1 mol. % N_2 and 0-0.28 mol. % CH_4. Calcite and siderite were identified among the solids in the type 4 multiphase FI (L-V-S) FI (Fig. 12) by Raman spectroscopy.

The confirmed presence of dense CO_2 and associated N_2 in the type 1 and 2 FI is among the most significant findings of the Raman spectroscopic study, because these gases are believed to be the major indicative components of the gold-bearing fluids in the studied area.

4.5. Crush-leach bulk analyses data

Quartz for crush-leach analysis was selected from least deformed samples. The method requires ~1 g mineral separates that allows reliable separation of an undeformed quartz variety. Results of crush-leach bulk analyses of fluid inclusions are presented in Table 3. Bulk analysis

data confirm the presence of carbon dioxide, chlorine, HCO_3^- ion, Na, K, Ca, Mg and some trace components in the fluid. The gold content in the bulk leachates reaches 18-131 ppm Au, exceeding the average ore grade. The bulk leachate data are consistent with the data on individual FI and show good agreement between corresponded anion/cation ratios (Table 4). The major cation is Na whereas the major anions are Cl^- and HCO_3^- ion. The inferred total concentrations of the solutes are also in good agreement with microthermometric data, indicating concentrations of 2.3-3.7 wt. % in Sukhoi Log, 1.4-2.5 wt. % in Verninsk, 10.4 wt. % in Uryakh and 25.5-41.1 wt. % in Irokinda solutions. The bulk analysis of the leachates reflects the contributions of FI of different type. However, CO_2 and N_2 are certainly contributed by two major gas-rich FI types: type 1 CO_2-aqueous and type 2 (V) inclusions. Therefore, we envisage that CO_2 and N_2 values in the crush-leach experiments are representative of the composition of ore-related fluid. The presence of a high Au concentration supports this conclusion.

5. C and N isotope compositions of fluid inclusion gases

The $\delta^{13}C_{CO2}$ isotope composition of gases in the fluid inclusions was measured in samples from all studied deposits in order to constrain the possible sources of the auriferous fluids (Plessen and Lüders, 2012). Although the different generations and fractions of heterogeneous fluids are trapped in the FI, the $\delta^{13}C_{CO2}$ values for the deposits fall into narrow ranges (Table 5).

Quartz from all the studied samples, except only samples from Irokinda, hosts gas-rich inclusions showing only negative $\delta^{13}C_{CO2}$ values in the range from -1.9 to -5.9 ‰ (Table 5). In contrast, gas-rich inclusions in quartz samples from the Irokinda deposit show both negative and positive $\delta^{13}C_{CO2}$ values in the narrow range between -0.6 and +0.6 ‰ (Table 5, Fig. 13). In addition to CO_2, traces of CH_4 and/or N_2 were detected in some of the samples (Table 5). Certain Sukhoi Log inclusions with high-density CO_2-N_2-bearing gas mixtures provided high N_2 gas inflow that allowed combining online measurements of both N_2 and CO_2 isotopic composition (Table 5). The measured $\delta^{15}N$ values vary from +3.0 to +5.9 ‰ (Table 5).

These results well agree with the previous findings (Lüders et al., 2015) on the relatively uniform C isotope compositions of CO_2 in the gases of fluid inclusions from orogenic deposits, which likely indicate the large-scale CO_2 supply from an isotopically homogeneous source. These CO_2-dominated gas signatures are suggested to be among the major indicative features of a fertile fluid systems in the area.

6. Discussion

6.1. Systematics of fluid chemical compositions

The large statistics of the study is still not sufficient with regard for the huge area of the gold-bearing provinces. However, certain provisional constraints on the sources of the mineralization can be suggested.

Ore-forming fluids of the Baikal–Patom gold deposits and the Uryakh deposit of Baikal-Muya are characterized by the relatively low salinity (1.4–9.5 wt.% NaCl equiv.) and the intermediate temperature. The high fluid pressure of 0.6-5.0 kbar corresponds to the lithostatic pressure for depths of 2-19 km that indicates a deep crustal origin of the fluid. The observed increase in the average pressure and temperature from the Sukhoi Log towards the Irokinda depositcorrelates with the positive shift of the C isotope compositions of CO2 in the fluid roughly from northwest to southeast (Fig. 14).

Our newly acquired data are in excellent agreement with earlier published microthemrometric data on fluid inclusions in quartz from Sukhoi Log, Uryakh and Irokinda (Lyakhov and Popivnyak, 1977; Laverov et al., 2000; Distler et al., 2004; Rusinov et al., 2008; Yudovskaya et al., 2016; Zlobina et al., 2016). The new data on the large Verninsk and small Dogaldyn deposits support the idea that gold mineralization of Baikal-Patom and Baikal-Muya was deposited from fluid rich in CO_2.

The gold deposits of these areas are regarded as orogenic deposits related to Paleozoic orogenesis and metamorphism (Distler et al., 2004; Goldfarb et al., 2014; Yudovskaya et al., 2016). The concept of orogenic-style mineralization includes the supply of gold by fluids under high-pressure from deep-seated (lower crustal) reservoirs (Cox, 2005). According to this concept, carbonic acid and low-salinity aqueous solutions, along with gold, are typical components of orogenic fluids (Phillips, 1993; Ridley and Diamond, 2000; Bodnar et al., 2014; et al.). Experimental evidence that CO_2 may act as a ligand for associated metals is absent so far, and it is generally thought that CO_2 does not form chemical species with Au, albeit CO_2 and Au accompany each other in metamorphic to orogenic processes (Lowenstern. 2001). Perhaps, CO_2 acts as a volatile agent in hydrothermal fluid and facilitates the unmixing and separation of a vapor phase. The latter can transport an appreciable amount of gold as sulfide or chloride complexes depending on temperature and fluid chemistry (Trigub et al., 2017; Zotov et al., 2017). Phillips and Powell (2010) suggested that aqueous-carbonic low-salinity orogenic fluid can efficiently dissolve and transport gold in the form of a gold-sulphide complex, with subsequent precipitation, but is not effective to dissolve sufficient amounts of base metals, which explains the general absence of base metals at orogenic deposits. The role of CO_2 can be also important at its percolation through gold-bearing hydrothermal aqueous solution (so-called gas barbotage), which promotes gold deposition due to a decrease in the amount of dense liquid, which is removed by the percolating gas phase (Prokofiev and Selector, 2014). The transport of

disperse gold nanoparticles by CO_2-rich gaseous fluid (Prokofiev et al., 2016) is also possible, whereas the subsequent mixing with aqueous fluid is suggested to result in gold precipitation. Therefore, although CO_2 itself does not play a role in gold transport, its involvement as a highly permeable substance creates a necessary conditions for gold scavenging and deposition. The important role of CO_2 in ore-forming processes at the Sukhoi Log deposit is supported by the CO_2-rich composition of gases trapped in the native gold, which hosts carbon dioxide, nitrogen, and methane without any traces of a liquid phase (Petrovskaya, 1973).

Three key papers overview substantial data on fluid inclusions in minerals from orogenic gold deposits worldwide (Ridley and Diamond, 2000, Bodnar et al., 2014, and Goldfarb and Groves, 2015). The compositions of fluids at Sukhoi Log, Verninsk, Dogaldyn and Uryakh are approximated by the H_2O–CO_2–NaCl system, with generally low salinities typical of orogenic fluids (Ridley and Diamond, 2000).

The fluids of the Irokinda deposit differ from fluids of the other studied deposits in having high temperatures, pressures and salinity (Figs. 10, 11). Bulk crush-leach data for the Irokinda deposit suggest that gold was precipitated from a fluid enriched in Cl, HCO_3^-, Br, Sr, Ba, Rb, Sb, Cs and Cd (Table 3). The presence of chloride and carbonate solids in the multi-phase type 4 fluid inclusions in Irokinda quartz supports the bulk crush-leach data (Table 4). Bodnar et al. (2014) argued that the range of the salinity of orogenic fluids can be much wider than that suggested in other overviews. Therefore, the Irokinda gas-rich brines also can belong to the orogenic type under these constraints (Bodnar et al., 2014).

Goldfarb and Groves (2015) discuss a possible modification of fluid compositions during the post-ore retrograde history of mineralization during cooling and decompression at exhumation, emphasizing that caution is required in interpreting FI data. While fluid overpressure during uplift may result in the expansion of FI and decrepitation, fluid underpressure may result in shrinkage and also in decrepitation, Sharing this opinion, we failed to find any evidence on superimposed fluid process that may affect the FI described above. We do accept the possibility of the formation of secondary inclusion at expense and by modification of primary ones, followed by CO_2 losses, but other effects on the largely preserved primary inclusions can be ruled out.

For the first time, we analyzed the gas composition of individual type 1 CO_2-aqueous and type 2 V FI in quartz from all the studied deposits by Raman spectroscopy. The analysis identifies N_2 as a predominant admixture in the CO_2-dominant gas phase and confirms our earlier detection of dense N_2 in fluid inclusions in quartz from productive gold-quartz-sulfide veinlets of the Sukhoi Log deposit (Dislter et al., 2004). The compositions of bulk fluids released at crushing of gold-bearing quartz are in good agreement with the compositions of the individual

FI, with both showing similar cation/anion ratios. The high Au content in bulk crush-leach samples add more confidence that the analyzed gas mixture is directly related to the ore-forming process.

6.2. Stable isotope constraints

The analysis of the stable isotope compositions of CO_2 and N_2 in fluids was aimed at defining the isotopic indicators of the possible sources of mineralizing fluids that can be of different provenance at the ore regareaion and at a given deposit (Goldfarb and Groves, 2015). For instance, Lowrence et al. (2013) identify a few different sources of orogenic fluids for the gold deposits in West Africa.

Direct measurements of the C isotopic compositions of CO_2 of the mineral-forming fluid trapped as fluid inclusions in quartz were also the first for all the studied deposits. The C isotopic composition of CO_2 from Sukhoi Log, Verninsk, Uryakh and Dogaldyn is characterized by the narrow range of $\delta^{13}C_{CO2}$ values varying from –1.9 to –5.9‰, whereas Irokinda quartz contains CO_2 with an even narrower range of $\delta^{13}C_{CO2}$ from +0.6 to –0.6 ‰ (Table 5, Fig. 13). Previous studies provided the C isotope compositions of Mg-Fe carbonates from quartz-sulfide and quartz-carbonate veins and veinlets of the Sukhoi Log deposits. The carbon of Sukhoi Log carbonates has a C isotope compositions ranging from -0.1 to -6.1 ‰ $\delta^{13}C$ according to Distler et al., 2004), from –3.8 to –5.9 ‰ according to Kryazhev et al. (2009), and from –4.6 to –9.2 ‰ according to the latest study by Dubinina et al., 2014. The variations in the C isotope composition of the fluid calculated from the $\delta^{13}C$ values of the carbonate are even wider, although both ranges are relatively narrow compared to the much broader range of -6.7 to -42 ‰ of the $\delta^{13}Corg$ values for organic carbon from the host black shales of Sukhoi Log (Distler et al., 2004).

The $\delta^{13}C_{CO2}$ range of –4.8 до –5.5 ‰ determined for FI in Sukhoi Log quartz are very close to the highest $\delta^{13}C$ values for Sukhoi Log carbonates. Dubinina et al. (2014) reported that carbonates in universalized host rocks have a C isotope composition in the range from –5.2 до –10.5 ‰ $\delta^{13}C_{CO2}$ and are depleted in the heavy C isotope compared to carbonates from the orebody. Therefore, we can state that the C isotope composition of CO_2 from FI corresponds to the primary isotope composition of mineralizing fluid, whereas the C isotope characteristics of carbonates from the ore veins reflect interaction between the fluid and the carbonate hosts. The textural relationships (Fig. 5) suggest that carbonate crystallization in the vein significantly postdates the crystallization of native gold. This post-ore fluid-rock interaction results in the wide variations of the C isotope compositions of carbonates.

The C isotope compositions of orogenic fluids are discussed in many papers and reviews (Kerrich, 1989; McCuaig and Kerrich, 1998 and references therein), which mention a rather wide range of -11 to +2 ‰ $\delta^{13}C$. Recently, based on the published data, Goldfarb and Groves (2015) suggested that the C isotope composition of orogenic fluids can vary more significantly within the range of -30 to +4.1 ‰. However, all reported data on the isotope compositions of fluids were obtained by recalculation of the isotope compositions of carbonates from mineralized rocks and veins. This approach may provide significant bias because carbonate deposition was not synchronous with but rather postdated gold mineralization, and the carbonate compositions reflect fluid-rock interaction at relatively low temperatures that resulted to the observed wide variations in their isotope characteristics. Therefore, we cannot compare our results of the direct measurements of the C_{CO2} isotope compositions with data obtained by the different approach.

This range of the carbon isotopic composition of gases in fluid inclusions from Sukhoi Log, Verninsk, Uryakh and Dogaldyn (–1.9 to –5.9‰ $\delta^{13}C$, (Fig. 13) can be interpreted to account for a magmatic (granitic) or even a mantle source of CO_2 (Hoefs, 2009). A magmatic source of gold-bearing fluids has been discussed in many previous studies (e.g. Sher, 1972; Rundqvist et al., 1992; Distler et al., 1996; Lishnevsky, Distler, 2004; Kucherenko et al., 2011; Yudovskaya et al., 2016). However, the origin of CO_2 from a mantle source can be ruled out due to the positive $\delta^{15}N$ values in high-density CO_2-N_2 inclusions in quartz (Fig. 15), because these values univocally suggest a crustal provenance of the N_2, although tehse data do not rule out sedimentary, metamorphic or magmatic crustal origins. However, the whole dataset is not consistent with that CO_2 (and gold) were scavenged and concentrated from the host rocks by metamorphic fluids, as was suggested in (Large et al., 2007; Dubinina et al., 2014; et al.).

The high carbonate concentrations in Irokinda fluids could be derived from marine limestones, a hypothesis supported by the CO_2 carbon isotopic composition of the fluids that varies from +0.6 to –0.6 ‰ $\delta^{13}C_{CO2}$ within the range typical of marine limestone decarbonization (e.g., Hoefs, 2009).

Conclusions

We suggested that only Irokinda fluid inclusions reveal identifiable characteristics of two distinct sources of orogenic fluid: (i) provisionally crustal magmatic and (ii) marine carbonates. The fluid compositions of all the giant to small deposits of Baikal-Patom and Baikal-Muya belt define a rougly north-south trend of the increasing temperature and pressure, which correlates with the enrichment in heavy C isotope (Fig. 14). The Irokinda and Sukhoi Log fluids are two end-members of this trend, whereas the other deposits show intermediate characteristics, which likely reflect another contribution of the marine source to the fluid compositions. The trend is in

a good agreement with the geological setting and the lithologies of the host rocks of the deposits, and the increase in the temperature and pressure also correlates with the metamorphic grades of the host rocks. If this trend is confirmed by future studies at other gold deposits and ore occurrences, then it can be interpreted as resulting from the same large-scale ore-forming event, which was possibly synchronous throughout the whole Baikal-Patom-Muya area

Acknowledgements

This work was supported by the RFBR (projects 17-05-01167-a and 17-05-00387-a).

References

Ananin, V.A., Bakhtin, V.I., Doroshkevich, G.I., Maurishnin, E.S., Minin, V.V., Mironov, A.G., Roshchektayev, P.A., Osokin, A.P., and Yavirskaya, T.F., 2000. Gold of Buryatiya. Book 1. Structural–metallogenic zoning. Geological structure of ore deposits. Resource estimate. Ulan-Ude. (in Russian).

Bodnar, R.J. and Vityk, M.O., 1994. Interpretation of microterhmometric data for H_2O–NaCl fluid inclusions, in Fluid Inclusions in Minerals: Methods and Applications, Ed. By Benedetto De Vivo and Maria Luce Frezzotti, Pontignano: Sienna, pp. 117–130.

Bodnar, R.J., Lecumberri-Sanchez, P., Moncada, D., and Steele-Maclnnes, P., 2014. Fluid inclusions in hydrothermal ore deposits. Reference Module in Earth Systems and Environmental Sciences. Treatise on Geochemistry, 2nd Edition, Elsevier, pp. 119–142.

Borisenko, A.S. 1977., Cryometric study of the salt composition of solutions in mineral-hosted gas–liquid inclusions in, Geol. Geofiz. 8, pp. 16–28 (in Russian).

Brown, P.E., 1989. Flincor: A microcomputer program for the reduction and investigation of fluid inclusion data, Am. Mineral., 74, pp. 1390–1393.

Bulgatov, A.N., and Gordiyenko, I.V., 1999. Terranes of the Baikal Highland and spatial distribution of gold deposits within them. Geologiya Rudnykh Mestorozhdeniy 41, pp. 230–240.

Burrows, D.A., Wood, P.C., Spooner, E.T.C., 1986. Carbon isotope evidence for a magmatic origin for Archean gold-quartz vein ore deposits. Nature 321, pp. 851–854.

Buryak, V.A., 1982. Metamorphism and ore-forming processes. Nauka, Moscow (in Russian).

Buryak, V.A., Khmelevskaya, N.M. 1997. Sukhoy Log: One of the world's largest gold deposit: Genesis, localization of ore, and prediction criteria. Dal'nauka, Vladivostok, p. 156 (in Russian).

Chugaev, A.V., Nosova, A.A., Abramov, S.S., Chernyshev, I.V., Bortnikov, N.S., Larionova, Y.O., Goltsman, Y.V., Moralev, G.V., Volfson, A.A. Early Permian stage of formation of

gold-ore deposits of northeastern Transbaikalia: isotope-geochronological (Rb-Sr and 39Ar-40Ar) data for the Uryakh ore field. Doklady Earth Sciences. 2015. T. 463. № 2. C. 855-859.

Collins, P.L.P., 1979. Gas hydrates in CO_2 bearing fluid inclusions and the use of freezing data for estimation of salinity, Econ. Geol., 74, pp. 1435–1444.

Cox S.F., 2005. Coupling between deformation, fluid pressures, and fluid flow in ore-producing hydrothermal systems at depth in the crust. Economic Geology 100th Anniversary Volume. Littleton, Colorado: Society of Economic Geologists, Inc., pp. 39-75.

Distler, V.V., Mitrofanov, G.L., Nemerov, V.K., Kovalenker, V.A., Mokhov, A.V., Semeikina, L.K., Yudovskaya, M.A., 1996. Modes of occurrence of the platinum group elements and their origin in the Sukhoi Log gold deposit (Russia). Geology of Ore Deposits 38 (6), pp. 413-428.

Distler, V.V., Yudovskaya, M.A., Mitrofanov, G.L., Prokof'ev, V.V., Lishnevsky, E.N., 2004. Geology, composition, and genesis of the Sukhoi Log noble metals deposit, Russia. Ore Geology Reviews 24, pp. 7-44.

Dubinina, E.O., Chugaev, A.V., Ikonnikova, T.A., Avdeenko, A.S., Yakushev, A.I., 2014. Sources and fluid regime of quartz–carbonate veins at the Sukhoi Log gold deposit, Baikal-Patom Highland. Petrology 22, pp. 329-358.

Goldfarb, R.J., Baker, T., Dube, B., Groves, D.I., Hart, C.J.R., Gosselin, P., 2005. Distribution, character, and genesis of gold deposits in metamorphic terranes. Economic Geology 100, pp. 407-450.

Goldfarb, R.J., Groves, D.I., 2015. Orogenic gold: Common or evolving fluid and metal sources through time. Lithos 233 pp. 2-26.

Goldfarb, R.J., Taylor, R.D., Collins G.S., Goryachev N.A., Orlandini O.F., 2014. Phanerozoic continental growth and gold metallogeny of Asia. Gondwana Research 25, pp. 48-102.

Groves, D.I., Goldfarb, R.J., Gebre-Mariam, M., Hagemann, S.G., Robert, F., 1998. Orogenic gold deposits: A proposed classification in the context of their crustal distribution and relationship to other gold deposit types. Ore Geology Reviews 13, pp. 7-27.

Hoefs J., 2009. Stable isotope geochemistry. Springer, p. 285.

Ivanov, A.I., 2014. Gold of the Baikal-Patom Highland (Geology, Mineralisation, Perspectives). TSNIGRI, Moscow, p. 215 (in Russian).

Ivanov, A.I., Livshits, V.I., Perevalov, O.V., et al., Dokembrii Patomskogo nagor'ya (Precambrian of the Patom Highland), Moscow: Nedra, 1995.

Kerkhof van den, A.M., 1988. The System CO_2-CH_4-N_2 in Fluid Inclusions: Theoretical Modeling and Geological Applications. Free University Press, Amsterdam.

Kerkhof van den, A.M., Touret, J.L.R., Kreulen, R., 1994. Juvenile CO_2 in enderbites of Tromøy near Arendal, southern Norway: a fluid inclusion and stable isotope study. Journal Metamorphic Geology 12, pp. 301–310.

Kerrich, R., 1989. Geochemical evidence on the sources of fluids and solutes for shear zone hosted mesothermal Au deposits. In: Bursnall, J.T. (Ed.), Mineralization and Shear Zones. Geological Association of Canada Short Course 6, pp. 129–197.

Kerrich, R., Fryer, B.J., King, R.W., Willmore, L.M., van Hees, E., 1987. Crustal outgassing and LILE enrichment in major lithosphere structures, Archean Abitibi greenstone belt: evidence for the source reservoirs from strontium and carbon isotope traces. Contribution to Mineralogy and Petrology 97, pp. 156–168.

Konstantinov M.M., 2010. Gold deposits of Russia. Akvarel, Moscow, p. 378 (in Russian).

Kröner, A., Kovach, V., Belousova, E., Hegner, E., Armstrong, R., Dolgopolova, A., Seltmann, R., Alexeiev, D.V., Hoffmann, J.E., Wong, J., Sun, M., Cai, K., Wang, T., Tong, Y., Wilde, S.A., Degtyarev, K.E., Rytsk, E., 2014. Reassessment of continental growth during the accretionary history of the Central Asian Orogenic Belt. Gondwana Research 25, pp. 103-125.

Kryazhev, S.G., Ustinov, V.I., Grinenko, V.A., 2009. Fluid regime at the Sukhoi Log gold deposit: isotopic evidence. Geochemistry International 47, pp. 1041-1049.

Kucherenko, I.V., Gavrilov, R.Yu., Martunenko, V.G., Verchozin, A.V., 2011. Petrological-geochemical features of wall-rock metasomatism at the Sukhoy Log gold deposit, Lena Area. Part 2. In: Petrology of wall-rock metasomatism, Proceedings of Tomsky Technical University, 320, pp. 28-37 (in Russian).

Large, R.R., Maslennikov, V.V., Robert, F., Danyushevsky, L., Chang, Z., 2007. Multistage sedimentary and metamorphic origin of pyrite and gold in the giant Sukhoy Log deposit, Lena Goldfield, Russia. Economic Geology 102, pp. 1233-1267.

Laverov, N.P., Prokof'ev, V.Yu., Distler, V.V., Yudovskaya, M.A., Spiridonov, A.M., Grebeshchikova, V.I., Matel, N.L., 2000. New data on conditions of ore deposition and composition of ore-forming fluids in the Sukhoy Log gold-platinum deposit. Doklady Earth Science 371, pp. 357-361.

Lawrence, D. M., Treloqr, P. J., Rankin, A. H,. Boyce, A., and Harbidge, P., 2013. A fluid inclusion and stable isotope study at the Loulo mining district, Mali, West Africa: Implications for multifluid sources in the generation of orogenic gold deposits. Economic Geology 108, pp. 229–257.

Lishnevsky, E.N., Distler, V.V., 2004. Deep structure of the earth's crust in the district of the Sukhoi Log gold-platinum deposit (Eastern Siberia, Russia) based on geological and geophysical data. Geology of Ore Deposits 46, pp. 76-90.

Lowenstern J.B. 2001. Carbon dioxide in magmas and implications for hydrothermal system. Mineralium Deposita. 36 490-502.

Lüders V., Klemd R., Oberthür T., Plessen B., 2015. Different carbon reservoirs of auriferous fluids in African Archean and Proterozoic gold deposits: Constraints from stable carbon isotopic compositions of quartz-hosted CO_2-rich fluid inclusions. Mineral. Deposita 50, pp. 449–454.

Lyakhov, Y.V., Popivnyak, I.V., 1977. O fisiko-khimicheskikh usloviyakh razvitiya zolotogo orudeneniya Severnoy Buryatii. Izvestiya Akademii nauk SSSR. Seriya geologicheskaya 6, pp. 5-17. (In Russian).

Mao, J.W., Zhang, Z., Wang, Y., Kerrich, R., 2003. Nitrogen isotope and content record of Mesozoic orogenic gold deposits surrounding the North China craton. Science in China (D) 46. pp. 231–245.

McCuaig, T.C., Kerrich, R., 1998. P–T–t–deformation-fluid characteristics of lode gold deposits: evidence from alteration systematics. Ore Geology Reviews 12, pp. 381–454.

Meffre, S., Large, R.R., Scott, R., Woodhead, J., Chang, Z., Gilbert, S.E., Danyushevsky, L.V., Maslennikov, V., Hergt, J.M., 2008. Age and pyrite Pb isotopic composition of the giant Sukhoi Log sediment-hosted gold deposit, Russia. Geochimica et Cosmochimica Acta 72, pp. 2377-2391.

Migachev, I.F., Karpenko, I.A., Ivanov, A.I., 2008. The Sukhoi Log gold deposit: reappraisal and estimation of the ore field and district. Otechestvennaya Geologiya 2, pp. 55-67 (in Russian).

Mitrofanov, G.L., 2006. Tectonic basis of the localization and formation of noble metal deposits in the Southern Surroundings of the Siberian Platform. Doctorate Dissertation at IGEM RAS, Moscow (in Russian).

Nemerov, V.K., 1989. Geochemical Specialization of the Late Precambrian black shales of the Baikal-Patom Highlands. PhD dissertation of the Vinogradov Institute of Geochemistry RAS. Irkutsk (in Russian).

Petrovskaya N. V. 1973. Native Gold. Nauka, Moscow (in Russian).

Phillips, G.N., 1993. Metamorphic fluids and gold. Mineralogical Magazine 57, 365–374.

Plessen, B., Lüders, V., 2012. Simultaneous measurements of gas isotopic compositions of fluid inclusion gases (N_2, CH_4, CO_2) using continuous-flow isotope ratio mass-spectrometry. Rap Comm Mass Spec 26, pp. 1157–1161.

Prokofiev, V.Yu., Akinfiev, N.N., Selektor, S.L., 2016. Gas Mixing with aqueous solution in the ore-forming hydrothermal process: an example of gold. Geochemistry International 54 (5), pp. 403–414.

Prokofyev, V. Yu., Naumov, V. B., 1987. Geochemical features of the mineralizing solutions at the Zyryanov sulfide-polymetallic deposit, Rudnyy Altay. Geochemistry International 24(10), pp. 50-74.

Prokofiev V.Yu., Selector S.L., 2014. Fluid inclusion evidence for barbotage and its role in gold deposition at the Darasun goldfield (eastern Transbaykalia, Russia). Cent. Eur. J. Geosci. 6 (2), pp. 131-138.

Ridley, J.R. and Diamond, L.W., 2000. Fluid chemistry of orogenic lode gold deposits and implications for genetic models, Gold in 2000. SEG Reviews 13 pp. 141–162.

Roedder, E., 1984. Fluid inclusions. Review in Mineralogy, vol. 12. Mineralogical Society of America.

Rundqvist, I.K., Bobrov, V.A., Smirnova, T.N., Cmirnov, M.Y., Danilova, M.Y., Ascheulov, A.A., 1992. Stages of formation of the Bodaibo ore district. Geology of Ore Deposits 34, pp. 3–15 (in Russian).

Rusinov, V.L., Rusinova, O.V., Kryazhev, S.G., Schegol'kov, Yu.V., Alusheva, E.I., Borisovsky, S.E., 2008. Wall-rock metasomatism of carbonaceous terrigenous rocks in the Lena gold district. Geology of Ore Deposits 50 (1), pp. 1-40.

Rytsk, E.Yu., Kovach, V.P., Yarmolyuk, V.V., Kovalenko, V.I., Bogomolov, E.S., Kotov, A.B., 2011. Isotopic structure and evolution of the continental crust in the East Transbaikalian segment of the Central Asian Fold belt. Geotectonics 45, pp. 349-377.

Safonov, Yu.G., 2006. Geological-genetic types of gold and gold-bearing deposits. In: Large and Super-Large Ore Deposits, vol. 2. IGEM RAS, Moscow, pp. 17-96 (in Russian).

Skuzovatov, S., Wang, K.-L., Dril, S., Lee, H.-Y., Iizuka, Y., 2019. Geochemistry, zircon U-Pb and Lu-Hf systematics of high-grade metasedimentary sequences from the South Muya block (northeastern Central Asian Orogenic Belt): Reconnaissance of polymetamorphism and accretion of Neoproterozoic exotic blocks in southern Siberia. Precambrian Research 321, pp. 34–53

Sher, S.D., 1972. Metallogeny of Gold. Nedra, Moscow, p. 256 (in Russian).

Taylor, B.E., 1986. Magmatic volatiles: isotopic variation of C, H, and S. In: Valley, J.W., Taylor, H.P. Jr, O'Neil, J.R. (Eds): Stable isotopes in high temperature geological processes. Reviews in Geology 16, pp. 185–225.

Thiery, R., Kerkhof, A.M., Dubessy, J., 1994. PTX properties of CH_4-CO_2 and CO_2-N_2 fluid inclusions: modeling for T<31 ° C and P < 400 bars. European Journal of Mineralogy 6, pp. 753-771.

Trigub, A. L.; Tagirov, B. R.; Kvashnina, K. O.; Lafuerza, S.; Filimonova, O. N.; Nickolsky, M. S., 2017. Experimental determination of gold speciation in sulfide-rich hydrothermal fluids under a wide range of redox conditions. Chemical Geology 471, 52−64.

Tsygankov, A.A., Matukov, D.I., Berezhnaya, N.G., Larionov, A.N., Posokhov, V.E., Tsyrenov, B.Ts, Khromov, A.A., Sergeev, S.A., 2007. Magma sources and stages of emplacement of the Late Paleozoic granitoids in the West Transbaikal Region. Geology and Geophysics 48, 156-180.

Wood, B.L., Popov, N.P., 2006. The giant Sukhoi Log gold deposit. Geology and Geophysics 47, pp. 315-341

Yakubchuk, A., Stein, H., Wilde, A., 2014. Results of pilot Re-Os dating of sulphides from the Sukhoi Log and Olympiada orogenic gold deposits, Russia. Ore Geology Reviews 59, pp. 21-28.

Yarmolyuk, V.V., Kovalenko, V.I., Kovach, V.P., Rytsk, E.Yu., Kozakov, I.K., Kotov, A.B., Salnikova, E.B., 2006. Early stages of the Paleoasian Ocean formation: Results of geochronological, isotopic, and geochemical investigations of Late Riphean and Vendian-Cambrian complexes in the Central Asian Fold Belt. Doklady Earth Sciences 411, pp. 1184–1189.

Yudovskaya M.A., Distler V.V., Prokofiev V.Yu., Akinfiev N.N. Gold mineralization and orogenic metamorphism in the Lena province of Siberia as assessed from Chertovo Koryto and Sukhoi Log deposits // . Geoscience Frontiers. 2016. V. 7. № 3. pp. 453–481.

Yudovskaya, M.A., Distler, V.V., Rodionov, N.V., Mokhov, A.V., Antonov, A.V., Sergeev, S.A., 2011. Relationship between metamorphism and ore formation at the Sukhoi Log gold deposit hosted in black slates from the data of U-Th-Pb isotopic SHRIMP-dating of accessory minerals. Geology of Ore Deposits 53, pp. 27-57 (in Russian).

Zlobina, T.M., Murashov, K.Yu., Kotov, A.A., 2014. Modeling the structural-dynamic conditions of Au-Q veins localization at the Irokinda deposit, Muya gold-bearing area. Geologiya I Mineralno-Syryevyye Resursy Sibiri, no 3, Part 2, pp. 55–61 (in Russian).

Zlobina, T.M., Petrov, V.A., Prokofyev, V.Yu., Kotov, A.A., Murashov, K.Yu., Volfson, A.A., 2016. Uryakhskoye gold field (NE Transbaikalia): Formation of structural assemblages in centroid-type seismic regime. Doklady Akadmii Nauk, vol. 470, no. 4, pp. 452–467.

Zotov A. V., Tagirov B. R., Koroleva L. A., and Volchenkov V. A. 2017 Experimental modeling of Au and Pt coupled transport by chloride hydrothermal fluids at 350–450°C and 500–1000 Bar. Geology of Ore Deposits 59 434-442.

Figure captions

Fig. 1. Location map of gold deposits in the Baikal-Patom and Muya areas, Siberia. The area of the study is marked with a square.

Fig. 2. Schematic geodynamic map of the Baikal–Patom and Baikal–Muya foldbelts (Bulgatov and Gordiyenko, 1999) with locations of the gold deposits discussed in text.

Fig. 3. Simplified geological maps of the Baikal–Patom gold deposits: Sukhoi Log, Verninsk and Dogaldyn.

Fig. 4. Morphology and textures of gold-bearing quartz and quartz-sulfide veins exposed in the open pits (a-b) and underground (c-e): a – Sukhoi Log, b – Verninsk, c – Dogaldyn, d – Uryakh, e – Irokinda.

Fig. 5. Mineral paragenetic sequences and associated types of FI of the main ore stage in the studied gold deposits.

Fig. 6. Simplified geological maps of the Baikal–Muya gold deposits (Uryakh and Irokinda).

Fig. 7. Native gold grains in quartz from the studied gold deposits: a – Sukhoi Log, b – Verninsk, c – Dogaldyn (in a polished section under reflected light), d – Uryakh, e – Irokinda.

Au – native gold, Q – quartz, Py – pyrite, Sph – sphalerite.

Fig. 8. Types of fluid inclusions in quartz as exemplified by the Irokinda samples: a-d – type 1 CO_2-aqueous FI (a, b - in quartz, a - +25 °C, b - +5 °C; c, d - in sphalerite, c - +25 °C, d - –10 °C); e, f - type 2 V gas-rich CO_2 FI (e - +25°C, f - –10°C); g-i - type 3 L-V FI; k-m - type 4 L-V-S multi-phase FI of chlorine brines.

L – aqueous solutions, V – gas phase, L CO_2 – liquid CO_2, S halite – halite crystal.

Fig. 9. Distribution of primary, pseudosecondary and secondary FI in gold-bearing quartz from the studied gold deposits:

a – primary type 1 CO_2–aqueous FI and secondary type 3 L-V FI in Sukhoi Log gold-bearing quartz, b – pseudosecondary type 1 CO_2-aqueous FI in Sukhoi Log gold-bearing quartz, c – primary type 1 CO_2–aqueous FI in Verninsk gold-bearing quartz; d – secondary type 3 L-V FI in Verninsk gold-bearing quartz; e – primary type 4 L-V-S FI of chloride brines in Irokinda gold-bearing quartz; f – an association of syngenetic primary type 1 CO_2–aqueous FI and primary type 2 V FI in Irokinda gold-bearing quartz.

Fig. 10. Diagrams of salinity vs. homogenization temperature of mineralizing fluids for the Baikal-Patom-Muya gold deposits. The maximum and minimum values for each type of FI are shown.

Fig. 11. Diagrams of homogenization temperature vs pressure of mineralizing fluids for the Baikal-Patom-Muya gold deposits.

Fig. 12. Raman spectra of solid phases in the Irokinda multi-phase fluid inclusion: calcite (1) and siderite (2), Locations of analytical points 1 and 2 are shown in the photograph, quartz lines are labeled with Q.

Fig. 13. Values of $\delta^{13}C_{CO2}$ for quartz-hosted fluid inclusions of the Baikal–Patom and Baikal–Muya gold deposits. The diagram also shows the typical ranges of the $\delta^{13}C$ values of crustal and mantle rocks (Taylor, 1986 and references therein; Burrows et al., 1986; Kerrich et al., 1987; Hoefs, 2009 and references therein). Data on fluid inclusions hosted in quartz from enderbite are given according to Van den Kerkhof et al. (1994).

Fig. 14. Correlation between C isotope composition of CO_2 and average temperature (a) and average pressure (b) of fluids from the Baikal-Patom-Muya gold deposits.

Fig. 15. Diagram of $\delta^{13}C_{CO2}$ vs $\delta^{15}N$ values for quartz-hosted fluid inclusions from the Sukhoi Log gold deposit (modified after Lüders et al., 2015). Ranges of the $\delta^{13}C$ and $\delta^{15}N$ values in crustal and mantle rocks are taken from Taylor (1986, and references therein); Burrow et al., 1986; Kerrich et al., 1987; Jingwen, 2003 and references therein; Hoefs 2009 and references therein.

Table 1. Parameters of the mineralizing fluids in quartz- and sphalerite-hosted fluid inclusions from gold deposit in the Baikal-Patom and Muya area, Siberia,.

Deposits (number of samples)	Incl. type, mineral	n*	*T*h \ºC	*T*eut \ºC	*T*m ice \ºC (NaCl)	*T*m CO_2 \ºC	*T*h CO_2 (N_2)\ºC	Hom. mode CO_2	*T*m Clatrate \ºC	C, Eq. mas% NaCl	C CO_2 \mol/ kg solution	*D,* \g/cm^3 (Middle)	*Pressure,* \ *bar*
Sukhoi Log (23)	1 P CO_2-aquas Q	283	210-385	-30 to -34	-4.6 to -7.5	-57.1 to -82.2	-19.9 to +10.5	L	6.2-12.4	5.0-8.1	1.8-7.6	0.82-1.09	640-2630
	2 P CO_2-aquas V Q	116	-	-	-	-57.0 to -60.8	-11.9 to +18.6	L	-	-	-	0.64-0.92 (0.81)	
	2a P V Q	252	-	-	-	-62.3 to -83.5	(-153.5 to -158.6)	V-L	-	-	-	0.12-0.57	-
	3 S L-V Q	403	130-385	-25 to -34	-2.2 to -7.5	-	-	-	-	3.7-9.5		0.65-0.97	-
Verninsk (5)	1 P CO_2-aquas Q	197	252-356	-25 to -32	-2.1 to -5.5	-57.1 to -60.8	-13.5 to +24.5	L	8.7-12.0	1.4-8.1	1.4-8.6	0.84-1.05	570-3150
	2 P V Q	33	-	-	-	-56.9 to -64.7	-13.7 to +30.8	L	-	-	-	0.54-1.00 (0.86)	
	1 PS CO_2-aquas Q	4	179	-31	-3.4	-58.0	28.5	L	7.8	5.0	2.3	1.03	-
	3 S L-V Q	34	136-261	-26 to -33	-3.1 to -3.9	-	-	-	-	5.0-6.2	-	0.83-0.97	-

Dogaldyn (6)	1 P CO_2-aquas Q	37	265-339	-30 to -39	-1.2 to -5.1	-56.8 to -60.2	-7.6 to +13.8	L	8.1-11.0	1.4-7.3	2.6-7.1	0.90-1.05	960-3230
	2 P V Q	122	-	-	-	-57.0 to -60.4	-14.1 to +22.1	L	-	-	-	0.70-1.02 (0.89)	
	1P CO_2-aquas Sph	8	267-283	-39	-5.1	-60.2	+11.4 to +13.3	L	8.6	6.7	3.7	1.05	-
	1 PS CO_2-aquas Q	15	128-236	-29 to -30	-2.5… -5.0	-	13.6 to 21.7	L-V	7.4-8.9	3.7-7.3	1.7-2.9	0.96-1.05	-
Uryakh (5)	1 P CO_2-aquas Q	25	289-361	-30 to -34	-4.8… -7.1	-57.3 to -58.0	-8.8 to +20.1	L	7.3-9.2	2.5-5.2	3.8-7.7	0.96-1.06	1050-3290
	2 P V Q	102	-	-	-	-57.0 to -59.1	-14.3 to +25.6	L	-	-	-	0.70-1.01 (0.88)	
	1 PS CO_2-aquas Q	4	213	-30	-6.6	-58.1	-30.9	L	7.3	5.2	3.8	1.08	-
	3 S L-V Q	8	191	-30	-5.9	-	-	-	-	9.1		0.94	-
Irokinda (10)	1 P CO_2-aquas Q	146	270-384	-30 to -52	-3.6 to (+10.8)	-57.0 to -62.6	-4.3 to +29.3	L	-10.0 to +14.8	3.9-23.4	2.4-7.7	0.98-1.15	840-5030
	2 P V Q	229	-	-	-	-56.7 to -61.0	-32.4 to +27.5	L	-	-	-	0.65-1.09 (0.90)	
	4 P L-V-S Q	19	320-453	-40… -55	(320-389)	-	-	-	-	39.8-46.3	-	1.02-1.13	

1 PS CO_2-aquas Q	3	191	-36	-5.9	-	29.0	L	6.8	8.5	1.5	1.06	-
1 P CO_2-aquas Sph	13	270	-32	-6.0 to -6.4	-62.6	-11.0 to -5.4	L	14.0-14.8	7.5	5.2	1.09	-
3 S L-V Q	60	179-230	-34 to -60	-8.0 to -15.3	-	-	-	-	11.7-18.9	-	0.97-1.03	-

Note: Inclusions type: 1 – CO_2-aquas, 2 – (V) vapor CO_2, 2a – (V) vapor N_2, 3 – L-V gas-liquid water-salt solutions, 4 – L-V-S chlorine brines; P – primary, PS – pseudosecondary, S – secondary. n* – number of inclusions. *Sph – inclusion in sphalerite. Q – quartz.
The table presents the maximum and minimum values for all microthermometric parameters for each type of inclusions.

Table 2. Raman data of molecular compositions of the gas phases of quartz-hosted fluid inclusions from gold deposits in the Baikal-Patom and Muya areas, Siberia (mol. %)

№ sample, FI	Type FI	CO_2	N_2	H_2S	CH_4
		Sukhoi Log			
8-202/3 1	2 V	80.2	19.7	0.00	0.03
8-202/3 2	2 V	74.4	25.6	0.00	0.00
		Verninsk			
V14-17 1	1 CO_2-aquas	92.9	7.1	0.00	0.01
V14-17 2	1 CO_2-aquas	91.5	8.5	0.00	0.00
V14-17 3	1 CO_2-aquas	91.4	8.6	0.00	0.00
V14-21 2	1 CO_2-aquas	89.2	10.8	0.00	0.00
V14-21 3	1 CO_2-aquas	96.3	3.7	0.00	0.00
V14-21 4	1 CO_2-aquas	98.4	1.6	0.00	0.00
V14-41 1	1 CO_2-aquas	77.7	22.2	0.04	0.02
P14-4 1	1 CO_2-aquas	98.3	1.7	0.00	0.02
P14-4 2	1 CO_2-aquas	92.0	8.0	0.00	0.04
P14-21 1	2 V	92.9	7.1	0.00	0.01
P14-41 2	2 V	91.8	8.2	0.00	0.00
P14-4 3	2 V	93.2	6.8	0.00	0.00
		Dogaldyn			
D14-22 1	2 V	99.0	1.0	0.00	0.00
D14-22 2	2 V	98.2	1.8	0.00	0.00
		Uryakh			
S-1 2	1 CO_2-aquas	98.2	1.8	0.00	0.00
S-1 1	2 V	96.1	3.9	0.00	0.00
		Irokinda			
1 2	1 CO_2-aquas	65.4	34.5	0.00	0.08
1 3	1 CO_2-aquas	56.6	43.4	0.00	0.04
15-32 2	1 CO_2-aquas	98.7	0.0	0.00	1.29
1 1	2 V	75.9	24.1	0.00	0.00
15-32 1	2 V	99.7	0.0	0.00	0.28
13a/12	2 V	99.4	0.6	0.00	0.01
13a/12	2 V	99.1	0.8	0.00	0.1

Table 3. Chemical composition of mineralizing fluids at gold deposits of the Baikal-Patom and Muya areas, Siberia

Deposits	Sukhoi Log		Verninsk		Uryakh	Irokinda	
Components	8/202.3	6/198.2	V10/32	V14/41	C 1	29/12	13b/12
				g/kg of H_2O			
CO_2	46.52	91.71	208.50	265.40	87.49	29.61	109.14
CH_4	0.018	0.99	0.181	0.157	0.09	5.34	0.07
Cl^-	0.99	1.22	1.24	1.24	17.25	78.52	43.29
HCO_3^-	15.15	25.39	16.47	8.56	55.19	203.92	133.22
Na	5.55	9.48	6.70	3.07	30.98	117.82	74.05
K	0.619	0.38	0.215	0.08	0.43	3.35	2.43
Ca	0.15	0.73	-	0.258	0.23	6.14	0.77
Mg	0.16	-	0.11	0.33	0.34	0.85	1.21
				ppm			
Br	34.6	464.3	460.4	84.8	331.8	4184.2	602.5
As	0.73	48.14	146.36	134.53	56.13	31.97	27.84
Li	11.40	57.40	16.13	26.55	0.12	0.13	0.31
B	7.47	2161.03	282.88	268.70	136.31	154.87	140.21
Rb	0.62	0.85	0.53	0.85	2.00	9.77	7.41
Cs	0.18	0.10	1.62	1.03	1.14	7.99	3.65
Sr	1.10	0.56	0.88	17.53	11.26	7516.5	119.33
Mo	5.97	16.41	0.09	-	0.07	0.15	0.09
Ag	7.14	82.99	0.12	1.86	0.14	0.03	0.02
Sb	0.07	1.42	38.88	8.85	15.05	58.73	10.01
Cu	2.44	79.41	-	-	0.43	0.07	6.59
Zn	240.84	89.32	7.02	14.32	3.59	30.39	307.41
Cd	0.11	0.15	0.19	-	-	0.04	3.33
Pb	2.00	0.78	-	0.22	0.59	-	19.47
Bi	0.18	0.05	0.01	-	0.03	0.02	-
Th	-	0.02	-		0.02	-	-
U	-	-	-	0.03	-	-	-
Ga			0.21	1.01	0.06	-	-
Ge	0.84	3.43	1.03	1.89	0.22	0.11	0.32
Sc	8.27	26.41	-	-	-	-	-

Ti	1.57	1.47	-	-	-	-	-
Mn	-	-	-	36.45	0.72	10.73	38.89
Fe	-	-	12.20	38.09	29.64	35.40	-
Co	0.11	1.80	0.17	0.30	0.01	0.07	0.49
Ni	12.50	14.55	0.60	5.81	0.69	2.14	2.22
V	-	-	3.21	0.92	0.91	1.02	0.32
Cr	0.84	-	0.21	0.71	0.08	0.18	-
Y	-	-	0.05	-	0.004	0.034	0.027
Zr	0.22	0.15	0.03	-	0.13	0.01	-
Sn	0.29	-	-	6.23	0.07	0.09	0.12
Ba	0.51	2.82	-	5.36	5.45	1640.0	280.86
W	1.68	4.16	0.73	0.37	1.00	1.26	0.13
Te	-	-	-	-	-	0.09	-
Au	0.020	0.049	0.124	0.031	0.018	-	0.038
Hg	0.36	0.71	-	-	0.05	0.29	0.12
Tl	0.03	0.17	0.01	0.02	0.02	0.09	0.15
REE	0.075	0.245	0.062	0.404	0.079	0.239	0.104
Ta	-	-	-	0.016	0.004	0.013	-
Na/K	9.0	25.0	31.2	39.3	72.6	35.2	30.5
CO_2 /CH_4	2584	93	1152	1690	1017	6	1495
K/Rb	1000	446	402	92	203	343	328

Table 4. Calculated cation and anion balance (mole fractions) and salinity (wt. %) in solutions at gold deposits of the Baikal-Patom and Muya areas, Siberia

Deposits	Sukhoi Log		Verninsk		Uryakh	Irokinda	
Element	8/202.3	6/198.2	V10/32	V14/41	C 1	13b/12	29/12
Na^+	0.90	0.97	0.97	0.86	0.98	0.96	0.95
K^+	0.06	0.02	0.02	0.01	0.01	0.02	0.01
Ca^{2+}	0.01	0.01	-	0.04	0.00	0.01	0.03
Mg^{2+}	0.02	-	0.01	0.09	0.01	0.01	0.01
Σ cations	0.99	1.00	1.00	1.00	1.00	1.00	1.00
Cl^-	0.10	0.08	0.12	0.20	0.35	0.36	0.40
HCO_3^-	0.90	0.92	0.88	0.80	0.65	0.64	0.60
Σ anions	1.00	1.00	1.00	1.00	1.00	1.00	1.00
Salinity, wt, %	2.3	3.7	2.5	1.4	10.4	25.5	41.1

Table 5. Stable carbon and nitrogen isotopic composition of gas-rich fluid inclusions in quartz from gold deposits of the Baikal-Patom and Muya areas, Siberia

Sample	Mineral	$\delta^{15}N_{N2}$	$\delta^{13}C_{CH4}$	$\delta^{13}C_{CO2}$
Sukhoi Log				
C 198.2	Quartz	5.9	n.d.	-5.5
22/262.1	Quartz	3.0	n.d.	-5.4
22/298.2	Quartz	3.8	traces	-5.0
8/204.9	Quartz	3.8	n.d.	-4.8
Verninsk				
V 10/32	Quartz	traces	n.d.	-1.9
V 14/17	Quartz	n.d.	n.d.	-3.4
V 14/21	Quartz	n.d.	n.d.	-2.9
V 14/41	Quartz	traces	n.d.	-4.1
P 14/4	Quartz	n.d.	n.d.	-3.2
Dogaldyn				
D 14/22	Quartz	traces	n.d.	-2.6
Uryakh				
C-1	Quartz	n.d.	n.d.	-2.9
C-5	Quartz	n.d.	n.d.	-2.6
Irokinda				
29/12	Quartz	n.d.	-36.0	-0.4
13B/12	Quartz	n.d.	n.d.	-0.6
I 27/15	Quartz	n.d.	n.d.	+0.1
I 32/15	Quartz	n.d.	n.d.	-0.3
I 3/15	Quartz	n.d.	n.d.	-0.4
I 15/15	Quartz	n.d.	n.d.	+0.6
I 32/15-1	Quartz	n.d.	n.d.	-0.3
I 15/32-2	Quartz	n.d.	n.d.	+0.6
I 6/15-3	Quartz	n.d.	n.d.	+0.5
I 32/15-2	Quartz	n.d.	n.d.	+0.6
I 32/15	Quartz	n.d.	n.d.	-0.3

Table 1. The parameters of the mineralizing fluids in fluid inclusions in quartz and sphalerite from the Baikal-Patom and Muya regions (Siberia) gold deposit.

Deposits (number of samples)	Incl. Type, mineral	n*	*T*h \ºC	*T*eut \ºC	*T*m ice \ºC (NaCl)	*T*m CO_2 \ºC	*T*h CO_2 (N_2)\ºC	Hom. mode CO_2	*T*m Clatrate \ºC
Sukhoi Log (23)	1 P CO_2-aquas Q	283	210-385	-30 to -34	-4.6 to -7.5	-57.1 to -82.2	-19.9 to +10.5	L	6.2-12.4
	2 P CO_2-aquas V Q	116	-	-	-	-57.0 to -60.8	-11.9 to +18.6	L	-
	2a P V Q	252	-	-	-	-62.3 to -83.5	(-153.5 to -158.6)	V-L	-
	3 S L-V Q	403	130-385	-25 to -34	-2.2 to -7.5	-	-	-	-
Verninsk (5)	1 P CO_2-aquas Q	197	252-356	-25 to -32	-2.1 to -5.5	-57.1 to -60.8	-13.5 to +24.5	L	8.7-12.0
	2 P V Q	33	-	-	-	-56.9 to -64.7	-13.7 to +30.8	L	-
	1 PS CO_2-aquas Q	4	179	-31	-3.4	-58.0	28.5	L	7.8
	3 S L-V Q	34	136-261	-26 to -33	-3.1 to -3.9	-	-	-	-
Dogaldyn (6)	1 P CO_2-aquas Q	37	265-339	-30 to -39	-1.2 to -5.1	-56.8 to -60.2	-7.6 to +13.8	L	8.1-11.0
	2 P V Q	122	-	-	-	-57.0 to -60.4	-14.1 to +22.1	L	-
	1P CO_2-aquas Sph	8	267-283	-39	-5.1	-60.2	+11.4 to +13.3	L	8.6
	1 PS CO_2-aquas Q	15	128-236	-29 to -30	-2.5… -5.0	-	13.6 to 21.7	L-V	7.4-8.9
Uryakh (5)	1 P CO2-aquas Q	25	289-361	-30 to -34	-4.8… -7.1	-57.3 to -58.0	-8.8 to +20.1	L	7.3-9.2
	2 P V Q	102	-	-	-	-57.0 to -59.1	-14.3 to +25.6	L	-
	1 PS CO_2-aquas Q	4	213	-30	-6.6	-58.1	-30.9	L	7.3
	3 S L-V Q	8	191	-30	-5.9	-	-	-	-

Irokinda (10)	1 P CO_2-aquas Q	146	270-384	-30 to -52	-3.6 to (+10.8)	-57.0 to -62.6	-4.3 to +29.3	L	-10.0 to +14.8
	2 P V Q	229	-	-	-	-56.7 to -61.0	-32.4 to +27.5	L	-
	4 P L-V-S Q	19	320-453	-40… -55	(320-389)	-	-	-	-
	1 PS CO_2-aquas Q	3	191	-36	-5.9	-	29.0	L	6.8
	1 P CO_2-aquas Sph	13	270	-32	-6.0 to -6.4	-62.6	-11.0 to -5.4	L	14.0-14.8
	3 S L-V Q	60	179-230	-34 to -60	-8.0 to -15.3	-	-	-	-

Note: Inclusions Type: 1 – CO_2-aquas, 2 – (V) vapor CO_2, 2a – (V) vapor N_2, 3 – L-V gas-liquid water-salt solutions, 4 – L-V-S chlorine brines; P – primary, PS – psevdo secondary, S – secondary. n* – number of inclusions. *Sph – inclusion in sphalerite. Q – quartz.
The table presents the maximum and minimum values for all microthermometric parameters for each type of inclusions.

Table 2. Raman data of molecular compositions of gas phases of fluid inclusions in quartz from the Baikal-Patom and Muya regions (Siberia) gold deposit (mol. %)

№ sample, FI	Type FI	CO_2	N_2	H_2S	CH_4
		Sukhoi Log			
8-202/3 1	2 V	80.2	19.7	0.00	0.03
8-202/3 2	2 V	74.4	25.6	0.00	0.00
		Verninsk			
B14-17 1	1 CO_2-aquas	92.9	7.1	0.00	0.01
B14-17 2	1 CO_2-aquas	91.5	8.5	0.00	0.00
B14-17 3	1 CO_2-aquas	91.4	8.6	0.00	0.00
B14-21 2	1 CO_2-aquas	89.2	10.8	0.00	0.00
B14-21 3	1 CO_2-aquas	96.3	3.7	0.00	0.00
B14-21 4	1 CO_2-aquas	98.4	1.6	0.00	0.00
B14-41 1	1 CO_2-aquas	77.7	22.2	0.04	0.02
П14-4 1	1 CO_2-aquas	98.3	1.7	0.00	0.02
П14-4 2	1 CO_2-aquas	92.0	8.0	0.00	0.04
B14-21 1	2 V	92.9	7.1	0.00	0.01
B14-41 2	2 V	91.8	8.2	0.00	0.00

П14-4 3	2 V	93.2	6.8	0.00	0.00
Dogaldyn					
Д14-22 1	2 V	99.0	1.0	0.00	0.00
Д14-22 2	2 V	98.2	1.8	0.00	0.00
Uryakh					
C-1 2	1 CO_2-aquas	98.2	1.8	0.00	0.00
C-1 1	2 V	96.1	3.9	0.00	0.00
Irokinda					
1 2	1 CO_2-aquas	65.4	34.5	0.00	0.08
1 3	1 CO_2-aquas	56.6	43.4	0.00	0.04
15-32 2	1 CO_2-aquas	98.7	0.0	0.00	1.29
1 1	2 V	75.9	24.1	0.00	0.00
15-32 1	2 V	99.7	0.0	0.00	0.28
13a/12	2 V	99.4	0.6	0.00	0.01
13a/12	2 V	99.1	0.8	0.00	0.1

Table 3. Chemical composition of mineralizing fluids of the Baikal-Patom and Muya regions (Siberia) gold deposit

Deposits	Sukhoi Log		Verninsk		Uryakh	Irokinda	
Components	8/202.3	6/198.2	V10/32	V14/41	C 1	29/12	13b/12
g/kg of H_2O							
CO_2	46.52	91.71	208.50	265.40	87.49	29.61	109.14
CH_4	0.018	0.99	0.181	0.157	0.09	5.34	0.07
Cl^-	0.99	1.22	1.24	1.24	17.25	78.52	43.29
HCO_3^-	15.15	25.39	16.47	8.56	55.19	203.92	133.22
Na	5.55	9.48	6.70	3.07	30.98	117.82	74.05
K	0.619	0.38	0.215	0.08	0.43	3.35	2.43
Ca	0.15	0.73	-	0.258	0.23	6.14	0.77
Mg	0.16	-	0.11	0.33	0.34	0.85	1.21
ppm							
Br	34.6	464.3	460.4	84.8	331.8	4184.2	602.5
As	0.73	48.14	146.36	134.53	56.13	31.97	27.84
Li	11.40	57.40	16.13	26.55	0.12	0.13	0.31

B	7.47	2161.03	282.88	268.70	136.31	154.87	140.21
Rb	0.62	0.85	0.53	0.85	2.00	9.77	7.41
Cs	0.18	0.10	1.62	1.03	1.14	7.99	3.65
Sr	1.10	0.56	0.88	17.53	11.26	7516.5	119.33
Mo	5.97	16.41	0.09	-	0.07	0.15	0.09
Ag	7.14	82.99	0.12	1.86	0.14	0.03	0.02
Sb	0.07	1.42	38.88	8.85	15.05	58.73	10.01
Cu	2.44	79.41	-	-	0.43	0.07	6.59
Zn	240.84	89.32	7.02	14.32	3.59	30.39	307.41
Cd	0.11	0.15	0.19	-	-	0.04	3.33
Pb	2.00	0.78	-	0.22	0.59	-	19.47
Bi	0.18	0.05	0.01	-	0.03	0.02	-
Th	-	0.02	-		0.02	-	-
U	-	-	-	0.03	-	-	-
Ga			0.21	1.01	0.06	-	-
Ge	0.84	3.43	1.03	1.89	0.22	0.11	0.32
Sc	8.27	26.41	-	-	-	-	-
Ti	1.57	1.47	-	-	-	-	-
Mn	-	-	-	36.45	0.72	10.73	38.89
Fe	-	-	12.20	38.09	29.64	35.40	-
Co	0.11	1.80	0.17	0.30	0.01	0.07	0.49
Ni	12.50	14.55	0.60	5.81	0.69	2.14	2.22
V	-	-	3.21	0.92	0.91	1.02	0.32
Cr	0.84	-	0.21	0.71	0.08	0.18	-
Y	-	-	0.05	-	0.004	0.034	0.027
Zr	0.22	0.15	0.03	-	0.13	0.01	-
Sn	0.29	-	-	6.23	0.07	0.09	0.12
Ba	0.51	2.82	-	5.36	5.45	1640.0	280.86
W	1.68	4.16	0.73	0.37	1.00	1.26	0.13
Te	-	-	-	-	-	0.09	-
Au	0.020	0.049	0.124	0.031	0.018	-	0.038
Hg	0.36	0.71	-	-	0.05	0.29	0.12
Tl	0.03	0.17	0.01	0.02	0.02	0.09	0.15
REE	0.075	0.245	0.062	0.404	0.079	0.239	0.104
Ta	-	-	-	0.016	0.004	0.013	-

Na/K	9.0	25.0	31.2	39.3	72.6	35.2	30.5
CO_2 /CH_4	2584	93	1152	1690	1017	6	1495
K/Rb	1000	446	402	92	203	343	328

Table 4. Calculation of cations and anions balance (mole fraction) and salinity (wt. %) of solution of the Baikal-Patom and Muya regions (Siberia) gold deposit

Deposits	Sukhoi Log		Verninsk		Uryakh	Irokinda	
Element	8/202.3	6/198.2	V10/32	V14/41	C 1	13b/12	29/12
Na^+	0.90	0.97	0.97	0.86	0.98	0.96	0.95
K^+	0.06	0.02	0.02	0.01	0.01	0.02	0.01
Ca^{2+}	0.01	0.01	-	0.04	0.00	0.01	0.03
Mg^{2+}	0.02	-	0.01	0.09	0.01	0.01	0.01
Σ cations	0.99	1.00	1.00	1.00	1.00	1.00	1.00
Cl^-	0.10	0.08	0.12	0.20	0.35	0.36	0.40
HCO_3^-	0.90	0.92	0.88	0.80	0.65	0.64	0.60
Σ anions	1.00	1.00	1.00	1.00	1.00	1.00	1.00
Salinity, wt, %	2.3	3.7	2.5	1.4	10.4	25.5	41.1

Table 5. Stable carbon and nitrogen isotopic composition of gas-rich fluid inclusions in quartz of the Baikal-Patom and Muya regions (Siberia) gold deposit

Sample	Mineral	$\delta^{15}N_{N2}$	$\delta^{13}C_{CH4}$	$\delta^{13}C_{CO2}$
Sukhoi Log				
C 198.2	Quartz	5.9	n.d.	-5.5
22/262.1	Quartz	3.0	n.d.	-5.4
22/298.2	Quartz	3.8	traces	-5.0
8/204.9	Quartz	3.8	n.d.	-4.8
Verninsk				
V 10/32	Quartz	traces	n.d.	-1.9
V 14/17	Quartz	n.d.	n.d.	-3.4
V 14/21	Quartz	n.d.	n.d.	-2.9
V 14/41	Quartz	traces	n.d.	-4.1

P 14/4	Quartz	n.d.	n.d.	-3.2
Dogaldyn				
D 14/22	Quartz	traces	n.d.	-2.6
Uryakh				
C-1	Quartz	n.d.	n.d.	-2.9
C-5	Quartz	n.d.	n.d.	-2.6
Irokinda				
29/12	Quartz	n.d.	-36.0	-0.4
13B/12	Quartz	n.d.	n.d.	-0.6
I 27/15	Quartz	n.d.	n.d.	+0.1
I 32/15	Quartz	n.d.	n.d.	-0.3
I 3/15	Quartz	n.d.	n.d.	-0.4
I 15/15	Quartz	n.d.	n.d.	+0.6
I 32/15-1	Quartz	n.d.	n.d.	-0.3
I 15/32-2	Quartz	n.d.	n.d.	+0.6
I 6/15-3	Quartz	n.d.	n.d.	+0.5
I 32/15-2	Quartz	n.d.	n.d.	+0.6
I 32/15	Quartz	n.d.	n.d.	-0.3

Gold mineralization of five Baikal-Patom to Baikal-Muya deposits was formed from heterogeneous H_2O-CO_2 fluid.

Among them, only Irokinda fluids contain high-temperature brines.

Carbon isotope composition of CO2 from fluid inclusions indicates a crustal granite-related source of orogenic fluid for four deposits.

Irokinda fluids are distinguished by a significant metamorphic contribution from decarbonated limestone.

Uryakh

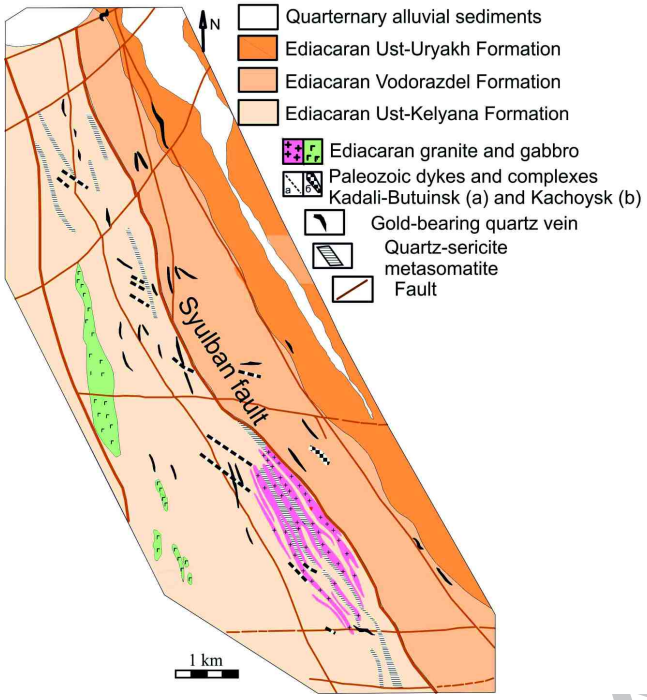

Irokinda

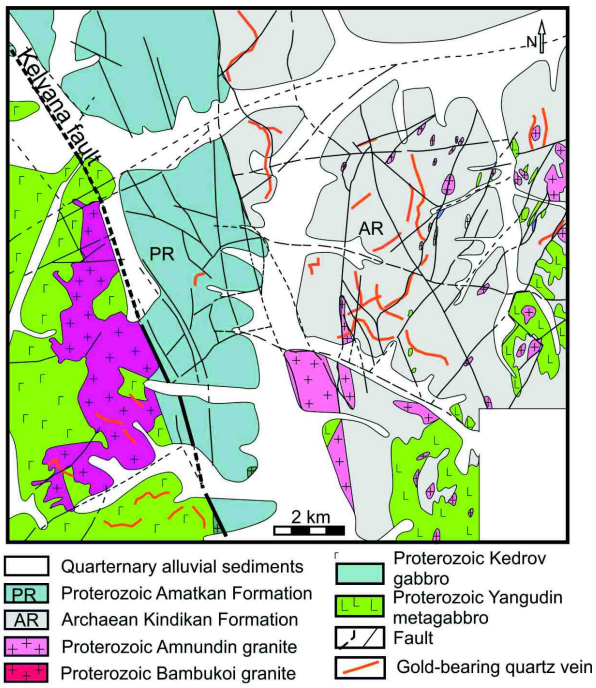

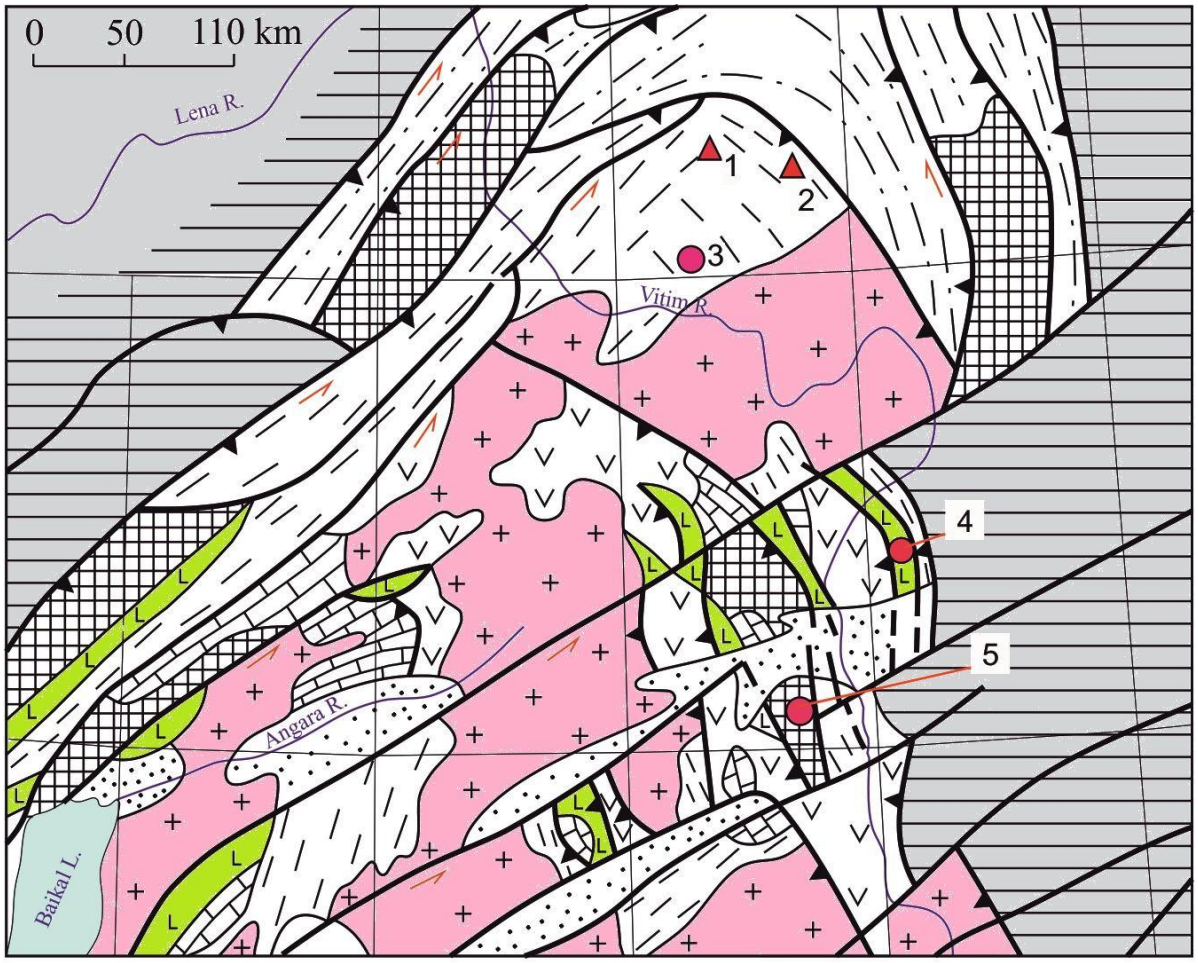

Siberian Craton

Patom fold-and-thrust belt

Cratonic terranes

Oceanic terranes

Island-arc terranes

Proterozoic turbidites sequences

Granites

Sedimentary rock

Cenozoic sediments

Thrusts and reverse faults

Gold deposits:
gold-quartz-sulfide (a),
gold-quartz (b)

1 – Sukhoi Log, 2 – Verninsk,
3 – Dogaldyn, 4 – Uryakh, 5 – Irokinda

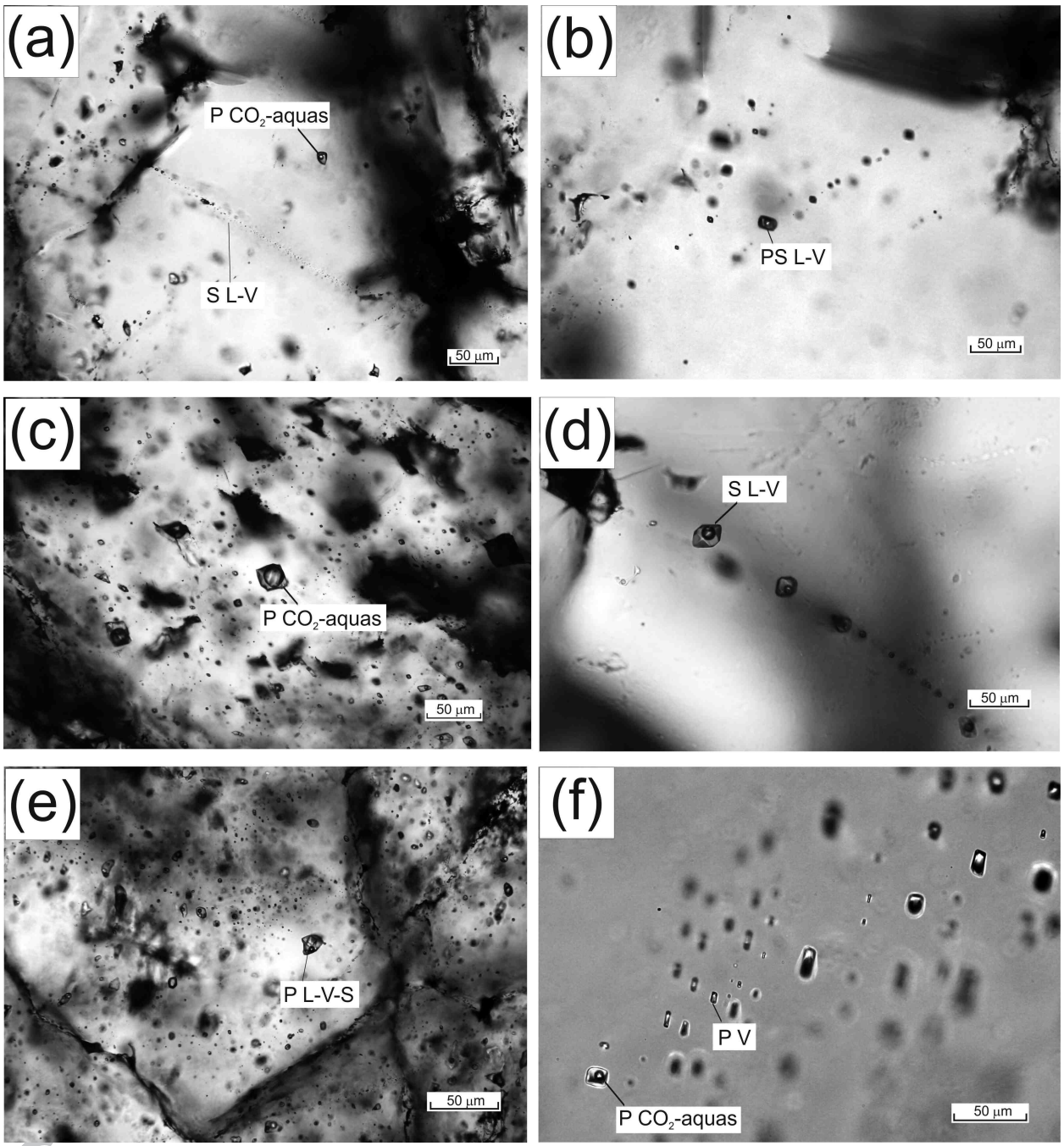

Sukhoi Log

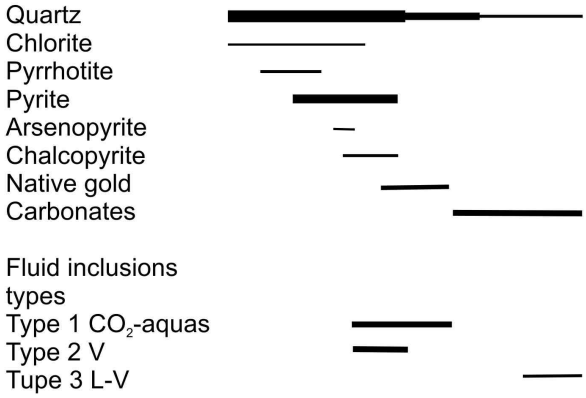

Verninsk

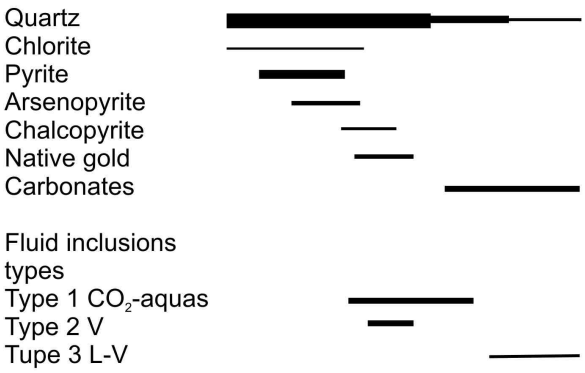

Dogaldyn

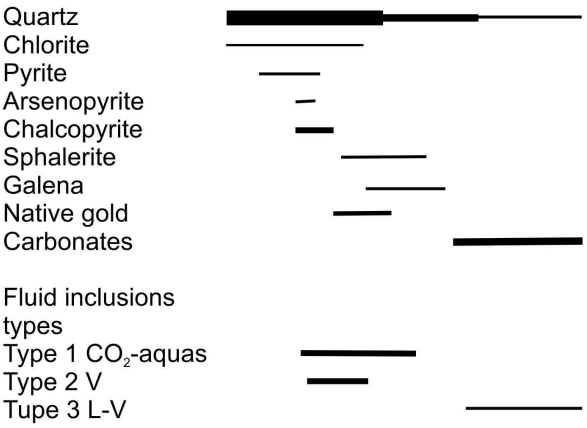

Uryakh

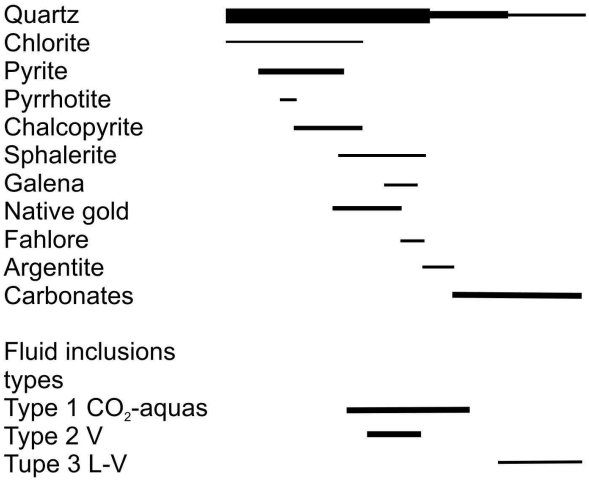

Irokinda